博 士 論 文

Behavior of Fluidized Particles and Plasma

in a DBD Plasma-enhanced Spouted Bed

噴流層型 DBD プラズマリアクターにおける

粒子とプラズマ挙動の解明

岐 阜 大 学

BAIQIANG ZHANG

2019.9

Doctoral thesis

博　士　論　文

Behavior of Fluidized Particles and Plasma

in a DBD Plasma-enhanced Spouted Bed

噴流層型 DBD プラズマリアクターにおける

粒子とプラズマ挙動の解明

BAIQIANG　ZHANG

張　百強

Gifu University，Environmental and Renewable Energy Systems

岐阜大学　工学研究科　環境エネルギーシステム専攻

2019.9

Abstract

Nowadays, many works so far have focused on the utilization of energy with high efficiency or for high-value production. Dielectric barrier discharge (DBD) plasma as the representational non-thermal plasma can be generated at atmospheric pressure with the advantages of highly transient, low-temperature, and non-equilibrium discharge. For the solid-particle systems, spouted bed reactor, as one typical type of the fluidized bed reactor, can be primarily proceeded for tiny particles and large particles in the industrial processes. Due to the capability of reforming certain useful cyclic operations, the spouted bed has been proposed to get over the comparatively random particle motion and unstable fluidization manner which is shown in a fluidized bed. In the past several decades, the combination of the fluidized/spouted bed reactor and non-thermal plasma irradiation technique has been played an essential role in the industrial chemical processes. It is feasible to use the effective conversion of electric field energy into the physical chemistry processes. However, the fundamental study of fluidization behavior for particles and plasma property in a plasma-enhanced spouted bed is poorly understood.

This study proposed a combination system of DBD plasma with a spouted bed reactor. DBD plasma was generated with an alternating current (AC) and a constant frequency of 20 kHz. The DBD plasma jet replaced the spouted bed jet, which contributed to the gas state changing to the plasma state. The parameters such as particle volume, particle type, and gas velocity which related to the fluidization situation of particles were changed. Besides, the effect of applied voltage and working gas, which affected the plasma generation were altered. The fluidization behavior of fine behavior, the fluid dynamic of large particles, and the effect of particles on the

plasma feature were investigated.

1)   Fluidization behavior of fine particles with plasma irradiation

To obtain the fluidization behavior of fine particles, we analyzed the minimum spouted velocity (u_{ms}) and pressure drop of white fused alumina (WA) particles with an average diameter of 58.6 μm under the plasma irradiation in a three-dimensional (3D) spouted bed. Essential operation parameters, such as static bed height, gas velocity, applied voltage, and working gas, were changed. The minimum spouted velocity, pressure drop, bed void fraction, and spouted bed temperature with the enhancement of plasma were measured.

As a result, the maximum value of the pressure drop of solid bed decreased and u_{ms} declined by the enhancement of applied voltage irrespective of the static bed height and type of working gas. The void fraction of solid bed was enhanced when the gas velocity less than the u_{ms}. It means the plasma irradiation improved the distance between particle and particle. Moreover, the entire solid bed was expanded not only the central part of the solid bed as a high voltage applied. Besides, even for a solid fixed bed with a low gas velocity, enhancing applied voltage leads the solid bed changed from a stable manner to spouted fluidization. Fluidization behavior varied with the working gas that the u_{ms} with N_2 was much higher than that of Ar at the same applied voltage. The temperature of the spouted bed and the particle surface did not show apparent changes when the voltage applied. The mechanism was proposed to show that the ionization of gas improved the interaction force between particles and may cause the minimum spouted velocity decreasing. The inherent interparticle forces (triboelectrification and Van der Waals) and interparticle forces

from the charge by the plasma irradiation, especially by repulsive force form the charge on the surface of WA particles (insulated particles) may be the main reason.

2)   DBD plasma property with particles addition

To gain an insight into the effect of fluidization behavior of particles on the characteristic of plasma in this combined system, we investigated the changes of optical emission spectroscopy (OES) for plasma with the fluidized polypropylene (PP) and black polypropylene (BPP, covered by the carbon material with a tiny layer) particles with a same diameter of 3 mm. Fluidization experiments with the DBD plasma irradiation were performed in a two-dimensional (2D) spouted bed. Essential operation parameters, such as particle type, applied voltage, gas velocity, and particle numbers, were changed. The pressure drop of particles, emission intensity of plasma, and high-speed camera images of the pattern was measured.

The pressure drop and u_{ms} of large particles had been decreased by the plasma irradiation, especially for PP particles. The emission spectra of Ar plasma had been changed significantly with particles. Due to the addition of PP particles, the emission intensity of the Ar I transition lines were increased, and Ar II lines were decreased. The emission intensities of Ar I lines were enhanced with the applied voltage regardless of the addition of particles. The emission intensity changed with the gas velocity versus particle numbers was identified with the fluidization behavior, that the emission intensity of plasma was increased with a gas velocity at first and then decreased for PP particles. The gas velocities corresponded to the highest values of emission intensity were similar to the trend of the changes of u_{ms} with various particle numbers. The

difference in the electrical conductivity and color of particles may affect the difference of pressure drop and detected emission intensity for two kinds of particles.

3) Fluid dynamics performance and mechanism for particles

To obtain the dynamic of solid particles with the irradiation of plasma. Particle velocity profiles were analyzed by the particle image velocimetry (PIV) and particle tracking velocimetry (PTV) methods. Several parameters included gas velocity, solid particle numbers, particle type (polypropylene (PP) and polyamide (PA)), and applied voltages were investigated here.

Results show that the particle velocity profile was increased especially at the longitudinal direction due to the plasma irradiation. The area of the highest particle velocity appeared at the upper part of the plasma inlet and expanded with 7 kV applied voltage regardless of gas velocity. With the increase of gas superficial velocity, the highest particle velocity area raised along the central line but not reached the surface of solid bed. The alters in emission intensity of plasma related to the fluidization behavior regardless of particle type. The electron temperature of Ar plasma decreased with the addition of particles. The charging mechanism had been proposed here that the enhancement of velocity due to the presence of two electric field (external electric field and surface charge electric field). Particle density and dielectric constant related to the difference of pressure drop and the enhancement of velocity.

This research extends the knowledge of the relationship between the fluidization behavior of particles and plasma optical characteristic. The promotion of plasma emission intensity by particles fluidization can provide a viable source for the chemical process, such as the process of plasmatic pollutant disposal with the catalysts. It suggests that the plasma irradiation changed the

fluidization behavior of solid bed, which c be used for the plasma process with a low-speed requirement. It is significant to control a good fluidization behavior for particles in the system because the electric field can be enhanced with the proper contact points and gap size between solid particles. It is well accepted that the optimal fluidization behavior of particles enhanced the plasma irradiation; on the other hand, the particle velocity was increased with the high applied voltage.

List of publication

Work published

[1]. 小林 信介，張 百強，花井 健吾，板谷 義紀. 噴流層プラズマリアクターを用いた 粒子表面改質[J]. 化学工学論文集，2018, 44 (4): 236–241.

[2]. Baiqiang Zhang, Nobusuke Kobayashi, and Yoshinori Itaya. Effect of plasma irradiation on the fine particle behavior in a spouted bed[J]. Powder Technology, 2019, 343: 309–316.

[3]. Baiqiang Zhang, Nobusuke Kobayashi, Yoshinori Itaya, Kyosuke Ono, and Akira Suami. Optical emission spectroscopy diagnostics of DBD plasma with particles in a two-dimensional spouted bed[J]. Chemical Engineering Science, 2019, 206: 31-40.

To be published

[1]. Baiqiang Zhang, Nobusuke Kobayashi, Yoshinori Itaya, Kyosuke Ono, Akira Suami, and Tsuguhiko Nakagawa. Fluid Dynamics Performance and Mechanism for Particles in an AC Dielectric Barrier Discharge Enhanced Spouted Bed.

Referred publication

[1]. Baiqiang Zhang, Guilin Piao, Jubing Zhang, Changsheng Bu, Hao Xie, Bo Wu, Nobusuke Kobayashi. Synthesis of carbon nanotubes from conventional biomass-based gasification gas[J]. Fuel Processing Technology, 2018, 180: 105-113.

Awards

1) 優秀ポスター賞，第 23 回流動化・粒子プロセッシングシンポジウム，2017.12.7. (Best poster presentation award, 23nd Fluidization & Particle Processing Symposium, 2017.12.7)

2) **最優秀学生賞,**化学工学会第 50 回秋季大会, プラズマシンポジウム,

2018.9.19. (Best student award, SCEJ 50th autumn meeting, 2018.9.19.)

International conferences

[1]. <u>Baiqiang Zhang</u>, Nobusuke Kobayashi, and Yoshinori Itaya. Behavior of Fine Particles in a Plasma-enhanced Spouted Bed[C]. The 7th Asian Particle Technology Symposium (APT 2017), 2017.7.30-8.3, Taiwan. (Oral report)

[2]. <u>Baiqiang Zhang</u>, Nobusuke Kobayashi, and Yoshinori Itaya. The Study of Fine Particle Behavior in a Plasma Enhanced Spouted Bed[C]. The 3rd NJNU-GIFU-ZJU Seminar on Clean Energy, 2017.9.27-28, Nanjing, China. (Oral report)

[3]. <u>Baiqiang Zhang</u>, Nobusuke Kobayashi, and Yoshinori Itaya. BEHAVIOR OF FINE PARTICLES IN A COLD PLASMA-ENHANCED SPOUTED BED[C]. 2017 AIChE Annual Meeting, 2017.10.29-11.03, Minneapolis, America. (Oral report)

[4]. <u>Baiqiang Zhang</u>, Nobusuke Kobayashi, and Yoshinori Itaya. Effect of particle fluidization behavior on the optical property of plasma in a plasma-enhanced spouted bed [C]. The 4th NJNU-GIFU-ZJU Seminar on Clean Energy, 2018.12.1, Nanjing, China. (Oral report)

[5]. <u>Baiqiang Zhang</u>, Nobusuke Kobayashi, and Yoshinori Itaya. Effect of particle properties on the characteristics of plasma in a DBD plasma enhanced spouted bed[C]. International Workshop on Environmental Engineering 2019, 2019.6.25-6.28, Okinawa, Japan. (Oral report)

Domestic conferences

[1]. <u>Baiqiang Zhang</u>, Nobusuke Kobayashi, and Yoshinori Itaya. Behavior of Fine Particles in a Plasma-enhanced Spouted Bed[C]. The 27th Symposium on Environmental Engineering. 2017.7.10-12, Hamamatsu, Japan. (Oral report)

[2]. <u>Baiqiang Zhang</u>, Nobusuke Kobayashi, and Yoshinori Itaya. Effect of Non-Thermal Plasma on the Fine Particle Behavior in a Spouted Bed[C]. 23nd Fluidization & Particle Processing Symposium, 2017.12.7-8, Hamamatsu, Japan. (Poster report)

[3]. <u>Baiqiang Zhang</u>, Nobusuke Kobayashi, and Yoshinori Itaya. Analysis of Fluidization Behavior for Fine Particles in a Non-Thermal Plasma-Enhanced Spouted[C]. Lecture Meeting of Tokai Branch of Nippon, Thermal Transaction Society of 2017, 2018.2.27, Gifu, Japan (Oral report)

[4]. <u>Baiqiang Zhang</u>, Nobusuke Kobayashi, Yoshinori Itaya, and Kyosuke Ono. Effect of Plasma Irradiation on Particle Dynamics in 2-D Spouted Bed[C]. SCEJ 50th autumn meeting, 2018.9.18－20, Kagoshima, Japan. (Oral report)

[5]. <u>Baiqiang Zhang</u>, Nobusuke Kobayashi, and Yoshinori Itaya. Effect of fluidization behavior on optical emission spectroscopy diagnostics of DBD plasma in a two-dimensional spouted bed[C]. 23nd Fluidization & Particle Processing Symposium, 2018.12.5-6, Hachioji, Japan. (Poster report)

Table of contents

List of abbreviations

Nomenclature

u_{ms}	minimum spouted velocity (m/s)
u_{mf}	minimum fluidization velocity (m/s)
u	gas velocity (m/s)
u_0	initial gas velocities (m/s)
n	ratio of u to u_{ms} (-)
$\triangle P$	pressure drop (Pa/kPa)
$\triangle P_{max}$	maximum value of pressure drop (Pa/kPa)
P_0	initial pressure drop (Pa)
H_0	static bed height of particles (mm)
$\triangle H$	height changes of the solid particles (mm)
U	applied voltage (kV)
f	frequency (kHz)
D_c	diameter of reactor (m)
D_i	inlet spout diameter (m)
T	temperature (°C)
T_e	electron temperature(°C)
t_0	initial residence time (s)
V	vectorial velocity (m/s)
V_y	vertical velocity (m/s)

V_x	horizontal velocity (m/s)
V_{max}	maximum value of vectorial velocity (m/s)
$V_{y\text{-}max}$	maximum value of vertical velocity (m/s)
$\overrightarrow{v_p}$	particle velocity (m/s)
m_p	mass of a particle (g)
$m_p g$	particle gravity (N)
F_d	drag force (N)
F_c	contact force (N)
F_E	electric field force (N)
E	electric field (N)

Greek Symbols

γ	spouted bed inlet angle (°)
φ	void fraction (-)
ρ_s	density of solid (kg/m^3)
ρ_g	density of gas (kg/m^3)
ρ_c	charge density of particles

Acronyms

2D	2-dimensional
3D	3-dimensional
CFD	computational fluid dynamics
DEM	discrete element method

TP	thermal plasma
NTP	non-thermal plasma
DC	direct current
AC	alternating current
DBD	dielectric barrier discharge
RF	radio frequency
MW	microwave
HCD	hollow cathode discharge
PIV	particle image velocimetry
PTV	particle tracking velocimetry
WA	white fused alumina
PP	polypropylene
BPP	black polypropylene
PA	polyamide
OES	optical emission spectroscopy
SEM	scanning electron microscopy
EI	emission intensity
EI_{max}	maximum value of emission intensity
EHD	electrohydrodynamic

1. Introduction

Nowadays, many kinds of research so far have focused on the utilization of energy with high efficiency or for high-value production. It is feasible to use the effective conversion of electric energy to the utilization in the physical chemistry processes on the gases or particles such as in the processes of pyrolysis/gasification and catalysis-assisted plasma system. This thesis proposes a combination system with a DBD plasma generator and spouted bed reactor. Two main contents will be researched in the whole thesis that is particles fluidization behavior and plasma feature in this combined system. In this chapter, the spouted bed process, as one type of gas-solid fluidization process, is introduced firstly. Further, various of non-thermal plasma processes are revealed here to indicate the possible utilization of dielectric barrier discharge (DBD) process. Moreover, the combination of plasma-enhanced fluidization process is reviewed. Besides, project aim and objectives are shown in the end.

1.1 Fluidization

Fluidization is a phenomenon that the solid particles can be fluidized in a reactor with force from gas or liquid. The gas-solid system with the fluidization is the most probable in the industrial processes. Fluidized bed reactor and spouted bed reactor are the main vessels. In the industrial processes, the fluidized bed reactor plays a vital role in a wide range of applications including pharmaceutical[1], agricultural products[2], and material processing[3] with the characteristics of the adequate mixing of the solid phase, high heat, and mass transfer rates[4].
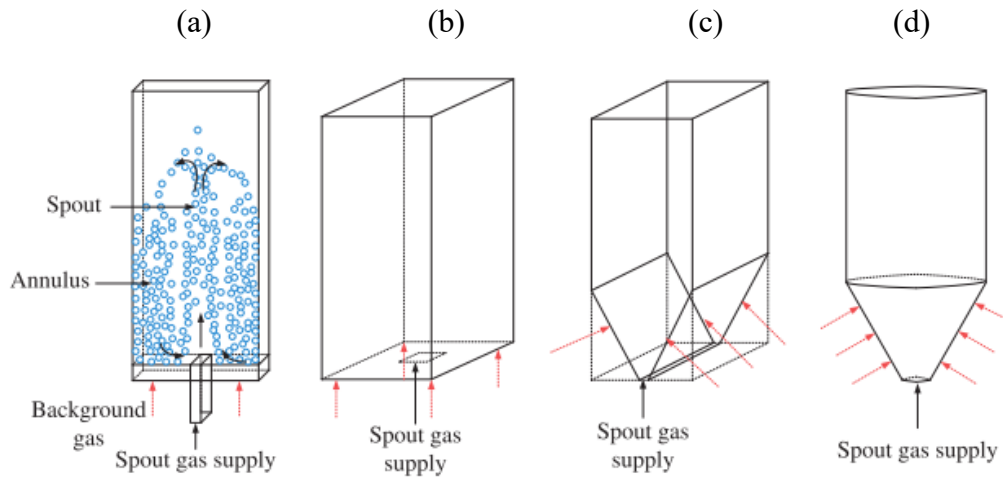
1.2 Spouted bed in energy and environment

Fig 1.1 Schematic of different spouted bed[4]

pseudo, (b) rectangular, (c)slotted rectangular, and (d) cylindrical.

(Black arrows indicate the spout gas flow and

red dotted arrows represent the background gas flow)

Spouted bed, one of the typical fluidized bed, is predominantly applied for solid-particle

systems using not only tiny particles (also called fine particles) but also very large particles,

which are difficult to fluidize stably. The high-velocity gas flows through an inlet from the bottom

of the spouted bed, which leads to the particles fluidized with a local high velocity along the

central axis and downflow along the bed walls. The details of the difference between a fluidized

bed and spouted bed can be found in Cui's review[5]. The spouted bed has been developed with

the capability of reforming certain useful cyclic operations[6] on the solid particles in the

chemical processes to overcome the comparatively random particle motion in a fluidized bed. A

combination of spouted fluidized bed also is developed as shown in Fig 1.1. Cylindrical (3-

dimensional,3D) and rectangular (2-dimensional, 2D) spouted beds have been drawn much

attention recently. To remove the "dead zone" in the bottom corner part of a rectangular spouted

bed, as shown in Fig 1.1(a) and (b), the background gas flow is needed. Conical bottom sections illustrated in Fig 1.1(c) and (d) can also well used without the background gas supplying also called as the 2-dimensional(2D) and 3-dimensional (3D) spouted bed.

Inlet gas properties (flow rate and density), particle properties (particle size, density, shape, and roughness) and spouted bed design (bed aspect ratio, shape, inlet angle, and dimension) affect the particle fluidization formation. Many pieces of researches on the fundamental fluidization behavior have been performed. Yang et al. [7] proposed a 2D spouted bed for assessing the behavior of the solids under six different flow patterns. He pointed out the formation of "curved gas path" appeared in the spouted bed and "stagnant region," which was occurred by particles accumulation along the conical inner walls. Panagiotis[8] verified the fine particles with an average diameter of 35 μm in a laboratory-scale spouted bed via hydrodynamic and simulation studies. Besides, the spouted bed is well used in the chemical industry processes primarily related to the environment and energy. The spouted bed had been proved as a fast and efficient method for the enteric coating to soft gelatin capsules in Pissinati's research[9]. He pointed out the coating efficiency direct proportion related to the ratio of feed mass flow rate of the coating suspension and the feed mass flow rate of spouting gas. Chen[10] verified a consistency of computational fluid dynamics-discrete element method (CFD-DEM) coupling simulation data and experimental data for mixing in a multiple-spouted bed. He clarified that the main factor to affect the particle mixing behavior was the density ratio of upper particles to lower particles. In the gasification of biomass process, even the particle size and roughness effect on the particle movement, but in Erkiaga's [11] research, the biomass particle size not effect obviously on the

gas composition and yields of tar and char that reduced the grinding of biomass to save an amount of energy. Fernandez-Akarregi[12] combined two spouted bed as the pyrolyzer and combustor in one system for heat integration in highly endothermic processes which can be used in the pyrolysis and gasification processes.

1.3 Plasma process

When the high temperature or a strong electric field added on the gas phase, the gas phase changed to the plasma state, which regarded as the fourth state of matter. Energetic particles included electrons, ions, and photons are the main constituents in plasma. Due to the reactive species of free radicals and metastable generated with plasma, plasma technique can be well used in the chemical processes. The heat, shock and acoustic wave, electrostatic, and electromagnetic fields have occurred as the transient fields with the plasma irradiation.

1.3.1 Non-thermal plasma

Depend on the temperature of electrons and other species, and atmospheric pressure plasma can be classified as thermal plasma (TP) and non-thermal plasma (NTP). For NTP generation process, the electrical energy replaces the enhancement of gas temperate to produce energetic matters, which results in a low-temperature of the whole plasma. So, the NTP is used in the physical and chemical processes with widespread applications. The main advantages of NTP plasma are highly transient, low-temperature, and non-equilibrium discharge[13] that allow it to initiate the formation of other various radicals with only a few degrees increase in temperature.

1.3.2 Types of NTP

Table 1.1   Classification of plasma actuators based on the frequency

Type	Frequency	Properties[14]	Typical discharge modes
DC discharge	Hz to kHz	voltage pulses in the kV range durations range from nanoseconds to microseconds	Glow discharge[15], Corona discharge [16], Arc discharge[17], DBD[18], Hollow cathode discharge (HCD)[19]
AC discharge	< 100 kHz	a sinusoidal voltage of a few kV in the 5–80kHz range	Glow discharge[20], Corona discharge[21], Arc discharge [22], DBD[23][24][25]
RF discharge	100 kHz ~ 100MHz	a standard RF source at 13.56MHz frequency	[26][27]
MW discharge	> 100MHz	based on a scaled-down version of a microwave plasma torch	[28][29]

The classification of NTP discharge based on the frequency (f) of applied voltage for exciting the discharge is illustrated in Table 1.1. Direct current (DC) discharge, alternating current (AC) discharge, radio frequency (RF) discharge, and microwave (MW) discharge are shown in the table. Based on the discharge property and discharge structure, the plasma also classified as the other modes, which are glow discharge, corona discharge, arc discharge, dielectric barrier discharge (DBD), and hollow cathode discharges (HCD).

1.3.3 DBD plasma characteristics

Among these plasma methods, DBD plasma is a representational non-thermal plasma process[30]. Compared to other plasma processes, DBD plasma can provide for a large-volume discharge at atmospheric pressure without the discharge's collapsing, which can be caused by the charge accumulation at the dielectric surface[31], into a constricted arc[32]. For decades it has aroused considerable attention in the field of industrial chemical processes[33][34][35][36], such as surface modification[37][38][39], coating[40], granulation[41], CO_2 dissociation[42], and pollutant removal[43][44] processes.

1.4 Combination of plasma and fluidization process

In industrial chemical processes, systems combined with plasma and fluidized particle have been studied for several years, but most of them were limited to the fundamental research and application process in fluidized beds. A microwave plasma-fluidized bed was developed by Matsukata [45]. Although the alumina and silicon particles had the same diameter of 150 μm, in the Ar condition, the minimum fluidization velocity (u_{mf}) of fine particles was decreased for alumina particles but without significant changes in the H_2 plasma system. Sathiyamoorthy[41] also determined that u_{mf} was less in a plasma-enhanced fluidized bed compared to a fluidized bed without the addition of plasma. Karches et al.[46] studied the coating process in a microwave plasma-enhanced circulating fluidized bed. Results revealed that the temperature of the process could be easily controlled to shallow values with similar electromagnetic properties. Zhu et al.[47] enhanced the removal efficiency by the combination of DBD plasma with MO_x/γ-Al_2O_3 catalysts

in a fluidized bed, and the formation of organic by-products was reduced. Pajkic et al.[48] developed a microwave plasma fluidized bed in a chemical vapor deposition process depositing a thin AlN coated on particulate substrates. Their process overcame the limitations posed by vacuum technology, such as high equipment capital and running costs.

Several studies related to applications in spouted beds with plasma irradiation have been performed. Tsukada et al.[49] investigated the granulation of spherical alloy grains from metal powder mixtures in a DC plasma-spouted/fluidized bed and grained spherical alloy 1–5 mm in diameter successfully within several minutes. Lee et al. [50] used a system that combined a gliding arc discharge with a spouted catalytic bed to investigate a plasma catalytic hybrid system for a CH_4 reforming process. Results showed that the distortion of discharge of the catalyst led to the decline of CH_4 conversion and a product's selectivity. The reactivity between excited gaseous species and the particles to be coated was improved in Sanchez's research [51] which enhanced the coating rate and decreased the mean operating temperature in a system with a gliding arc and spouted bed.

Based on the literature, there so many considerable applications can be used for this combination process, such as in the environmental application, material processing, the thermal sensitivity process—mendicant processing and energy applications.

1.5 Project aim and objectives

This thesis aims at the fundamental research proposed in a DBD plasma-enhanced spouted bed to achieve the particle fluidization behavior with the plasma irradiation in a spouted bed and

obtain the effect of the presence of particles on the plasma properties in the spouted bed reactor. This research will extend our knowledge on the relationship between plasma irradiation and the fluid dynamics in this combination system.

The main objectives of this thesis are as follows:

1)   Propose a combination system with AC DBD plasma and two types of spouted bed (3D and 2D).

2)   Obtain the fluidization behavior of fine particles and large particles by analyzing the pressure drop, void fraction, and calculating the minimum spouted velocity (u_{ms}).

3)   Analyze the emission intensity of plasma to get a relationship between particle fluidization behavior and plasma property.

4)   Perform particle image velocimetry (PIV) and particle tracking velocimetry (PTV) methods to obtain the velocity profile of large particle in the plasma-enhanced spouted bed.

5)   Explore the mechanism for the relation of particles fluidization behavior and plasma property.

1.6 Thesis structure

This thesis will be divided with the following parts:

Chapter 1. Here, the basic fluidization process is reviewed to go though the fluidized and spouted bed reactors in the chemical processes. Besides, the basic plasma techniques which are drawn much attention recently are presented. The literature review and considerable application of the combination with fluidization process and plasma technique are revealed at the end of this

chapter.

Chapter 2. This chapter presents the experimental set-up for this combination system with the two types of spouted bed reactor by showing the equipment schematic and the analysis methods which will be used.

Chapter 3. The fluidization behavior will be researched for fine particles in this chapter. The effects of particle volume, applied voltage, and working gases on the behavior of fine particles were investigated in a 3D spouted bed. The pressure drop and void fraction of the solid bed were measured, and minimum spouted velocity (u_{ms}) was calculated to understand the fluidization behavior of fine particles.

Chapter 4. This chapter focuses on investigating the effect of particles fluidization behavior on the optical emission spectroscopy diagnostics of the DBD plasma in a 2D spouted bed. In the experiment, several parameters were changed, including gas flow rate and particle numbers (fluidization parameter), applied voltages (plasma parameter), and particle type (surface material). The optical emission spectral characteristics and the effect of fluidization behavior on the emission intensity of Ar plasma were obtained.

Chapter 5. To investigate the effect of plasma irradiation on the particle movement dynamic, we changed several parameters, including gas flow rate and particle numbers (fluidization parameter), applied voltages (plasma parameter). The effect of plasma irradiation on the fluid dynamics was obtained by the particle image velocimetry (PIV) and particle tracking velocimetry (PTV) methods.

Chapter 6. Conclusion of this thesis.

1.7 References

[1].G. Kulah and O. Kaya, "Investigation and scale-up of hot-melt coating of pharmaceuticals in fluidized beds," Powder Technology, vol. 208, no. 1. pp. 175–184, 2011.

[2].S. R. L. Werner, J. R. Jones, A. H. J. Paterson, R. H. Archer, and D. L. Pearce, "Air-suspension coating in the food industry: Part II - micro-level process approach," Powder Technology, vol. 171, no. 1. pp. 34–45, 2007.

[3].G. K. Reynolds, J. S. Fu, Y. S. Cheong, M. J. Hounslow, and A. D. Salman, "Breakage in granulation: A review," Chem. Eng. Sci., vol. 60, no. 14, pp. 3969–3992, 2005.

[4].V. S. Sutkar, N. G. Deen, and J. A. M. Kuipers, "Spout fluidized beds: Recent advances in experimental and numerical studies," Chem. Eng. Sci., vol. 86, pp. 124–136, 2013.

[5].H. Cui and J. R. Grace, "Spouting of biomass particles: A review," Bioresour. Technol., vol. 99, no. 10, pp. 4008–4020, Jul. 2008.

[6].K. Mather, Spouted Beds. Elsevier Science, 1974.

[7].J. Yang, R. W. Breault, J. M. Weber, and S. L. Rowan, "Determination of flow patterns by a novel image analysis technique in a rectangular spouted bed," Powder Technol., vol. 334, pp. 151–162, 2018.

[8].P. N. Kechagiopoulos, S. S. Voutetakis, and A. A. Lemonidou, "Cold flow experimental study and computer simulations of a compact spouted bed reactor," Chemical Engineering and Processing: Process Intensification, vol. 82. pp. 137–149, 2014.

[9].R. Pissinati and W. P. Oliveira, "Enteric coating of soft gelatin capsules by spouted bed: effect of operating conditions on coating efficiency and on product quality," Eur. J. Pharm.

Biopharm., vol. 55, no. 3, pp. 313–321, May 2003.

[10]. M. Chen et al., "A novel mixing index and its application in particle mixing behavior study in multiple-spouted bed," Powder Technol., vol. 339, pp. 167–181, 2018.

[11]. A. Erkiaga, G. Lopez, M. Amutio, J. Bilbao, and M. Olazar, "Influence of operating conditions on the steam gasification of biomass in a conical spouted bed reactor," Chemical Engineering Journal, vol. 237. pp. 259–267, 2014.

[12]. R. Fernandez-Akarregi, J. Makibar, G. Lopez, M. Amutio, H. Altzibar, and M. Olazar, "Development of a dual conical spouted bed system for heat integration purposes," Powder Technology, vol. 268, no. 1. pp. 261–268, 2014.

[13]. V. I. Gibalov and G. J. Pietsch, "Development of dielectric barrier discharges in gas gaps and on surfaces," J. Phys. D. Appl. Phys., vol. 33, no. 20, pp. 2618–2636, 2000.

[14]. R. Zaplotnik et al., "Multiple vs. Single harmonics AC-driven atmospheric plasma jet," Epl, vol. 106, no. 2, 2014.

[15]. V. E. Fortov, A. P. Nefedov, V. I. Molotkov, M. Y. Poustylnik, and V. M. Torchinsky, "Dependence of the dust-particle charge on its size in a glow-discharge plasma," Phys. Rev. Lett., vol. 87, no. 20, pp. 205002-1-205002–4, 2001.

[16]. E. Moreau, L. Léger, and G. Touchard, "Effect of a DC surface-corona discharge on a flat plate boundary layer for air flow velocity up to 25 m/s," J. Electrostat., vol. 64, no. 3–4, pp. 215–225, 2006.

[17]. M. Liao, Y. Wang, H. Wu, H. Li, and W. Xia, "Study of Non-Thermal DC Arc Plasma of CH_4 /Ar at Atmospheric Pressure Using Optical Emission Spectroscopy and Mass

Spectrometry," Plasma Sci. Technol., vol. 17, no. 9, pp. 743–748, 2015.

[18].E. Moreau, R. Sosa, and G. Artana, "Electric wind produced by surface plasma actuators: A new dielectric barrier discharge based on a three-electrode geometry," J. Phys. D. Appl. Phys., vol. 41, no. 11, 2008.

[19].N. Sismanoglu, J. Amorim, J. A. Souza-Corrêa, C. Oliveira, and M. P. Gomes, "Optical emission spectroscopy diagnostics of an atmospheric pressure direct current microplasma jet," Spectrochim. Acta - Part B At. Spectrosc., vol. 64, no. 11–12, pp. 1287–1293, 2009.

[20].Li et al., "CO_2 reforming of CH_4 by atmospheric pressure glow discharge plasma: A high conversion ability," Int. J. Hydrogen Energy, vol. 34, no. 1, pp. 308–313, 2009.

[21].X. Tu and J. C. Whitehead, "Plasma dry reforming of methane in an atmospheric pressure AC gliding arc discharge: Co-generation of syngas and carbon nanomaterials," Int. J. Hydrogen Energy, vol. 39, no. 18, pp. 9658–9669, 2014.

[22].Y. Wang, H. Yu, C. Chen, and Z. Zhao, "Review of the biocompatibility of micro-arc oxidation coated titanium alloys," Mater. Des., vol. 85, pp. 640–652, 2015.

[23].Y. Sung, W. Kim, M. G. Mungal, and M. A. Cappelli, "Aerodynamic modification of flow over bluff objects by plasma actuation," Exp. Fluids, vol. 41, no. 3, pp. 479–486, 2006.

[24].S. B. Olenici-Craciunescu et al., "Characterization of a capillary dielectric barrier plasma jet for use as a soft ionization source by optical emission and ion mobility spectrometry," Spectrochim. Acta - Part B At. Spectrosc., vol. 64, no. 11–12, pp. 1253–1258, 2009.

[25].T. C. Corke, M. L. Post, and D. M. Orlov, "SDBD plasma enhanced aerodynamics: concepts, optimization and applications," Prog. Aerosp. Sci., vol. 43, no. 7–8, pp. 193–217, 2007.

[26].F. Piallat, C. Vallée, R. Gassilloud, P. Michallon, B. Pelissier, and P. Caubet, "PECVD RF versus dual frequency: An investigation of plasma influence on metal-organic precursors' decomposition and material characteristics," J. Phys. D. Appl. Phys., vol. 47, no. 18, 2014.

[27].S. Sridhar, L. Liu, E. W. Hirsch, V. M. Donnelly, and D. J. Economou, "Insights into the mechanism of in-plasma photo-assisted etching using optical emission spectroscopy," J. Vac. Sci. Technol. A Vacuum, Surfaces, Film., vol. 34, no. 6, p. 61303, 2016.

[28].G. S. Ho, H. M. Faizal, and F. N. Ani, "Microwave induced plasma for solid fuels and waste processing: A review on affecting factors and performance criteria," Waste Manag., vol. 69, pp. 423–430, 2017.

[29].Czylkowski, B. Hrycak, M. Jasiński, M. Dors, and J. Mizeraczyk, "Microwave plasma-based method of hydrogen production via combined steam reforming of methane," Energy, vol. 113, no. 2016, pp. 653–661, 2016.

[30].N. Benard and E. Moreau, "Electrical and mechanical characteristics of surface AC dielectric barrier discharge plasma actuators applied to airflow control," Exp. Fluids, vol. 55, no. 11, 2014.

[31].U. Kogelschatz, "Filamentary, patterned, and diffuse barrier discharges," IEEE Trans. Plasma Sci., vol. 30, no. 4 I, pp. 1400–1408, 2002.

[32].C. L. Enloe et al., "Mechanisms and Responses of a Dielectric Barrier Plasma Actuator: Geometric Effects," AIAA J., vol. 42, no. 3, pp. 595–604, 2004.

[33].J. J. Wang, K. S. Choi, L. H. Feng, T. N. Jukes, and R. D. Whalley, "Recent developments in DBD plasma flow control," Prog. Aerosp. Sci., vol. 62, pp. 52–78, 2013.

[34].R. Erfani, H. Zare-Behtash, C. Hale, and K. Kontis, "Development of DBD plasma actuators: The double encapsulated electrode," Acta Astronaut., vol. 109, pp. 132–143, 2015.

[35].Q. Wang, Y. Cheng, and Y. Jin, "Dry reforming of methane in an atmospheric pressure plasma fluidized bed with Ni/γ-Al$_2$O$_3$ catalyst," Catalysis Today, vol. 148, no. 3–4. pp. 275–282, 2009.

[36].L. H. Song, S. H. Park, S. H. Jung, S. D. Kim, and S. Bin Park, "Synthesis of polyethylene glycol-polystyrene core-shell structure particles in a plasma-fluidized bed reactor," Korean Journal of Chemical Engineering, vol. 28, no. 2. pp. 627–632, 2011.

[37].M. Sachs, J. Schmidt, W. Peukert, and K. E. Wirth, "Treatment of polymer powders by combining an atmospheric plasma jet and a fluidized bed reactor," Powder Technol., vol. 325, pp. 490–497, 2018.

[38].X. Zheng, G. Chen, Z. Zhang, J. Beem, S. Massey, and J. Huang, "A two-step process for surface modification of poly(ethylene terephthalate) fabrics by Ar/O$_2$ plasma-induced facile polymerization at ambient conditions," Surf. Coatings Technol., vol. 226, pp. 123–129, 2013.

[39].X. J. Shao, G. J. Zhang, J. Y. Zhan, and G. M. Xu, "Research on surface modification of polytetrafluoroethylene coupled with argon dielectric barrier discharge plasma jet characteristics," IEEE Trans. Plasma Sci., vol. 39, no. 11 PART 2, pp. 3095–3102, 2011.

[40].M. Karches and P. R. Von Rohr, "Microwave plasma characteristics of a circulating fluidized bed-plasma reactor for coating powders," Surface and Coatings Technology, vol. 142–144. pp. 28–33, 2001.

[41].Sathiyamoorthy, "Plasma spouted/fluidized bed for materials processing," J. Phys. Conf.

Ser., vol. 208, no. 1, p. 12120, Feb. 2010.

[42].Michielsen et al., "CO$_2$ dissociation in a packed bed DBD reactor: First steps towards a better understanding of plasma catalysis," Chem. Eng. J., vol. 326, pp. 477–488, 2017.

[43].Jõgi, K. Erme, J. Raud, and M. Laan, "Oxidation of NO by ozone in the presence of TiO$_2$ catalyst," Fuel, vol. 173, no. x, pp. 45–54, 2016.

[44].B. Sretenovi, "A dual-use of DBD plasma for simultaneous NO$_x$ and SO$_2$ removal from coal-combustion flue gas," vol. 185, no. x, pp. 1280–1286, 2011.

[45].M. Matsukata, K. Suzuki, K. Ueyama, and T. Kojima, "Development of a microwave plasma-fluidized bed reactor for novel particle processing," Int. J. Multiph. Flow, vol. 20, no. 4, pp. 763–773, Sep. 1994.

[46].M. Karches, C. Bayer, and P. Rudolf Von Rohr, "A circulating fluidised bed for plasma-enhanced chemical vapor deposition on powders at low temperatures," Surface and Coatings Technology, vol. 116–119. pp. 879–885, 1999.

[47].X. Zhu, X. Gao, X. Yu, C. Zheng, and X. Tu, "Catalyst screening for acetone removal in a single-stage plasma-catalysis system," Catalysis Today, vol. 256, no. P1. pp. 108–114, 2015.

[48].Z. Pajkic and M. Willert-Porada, "Atmospheric pressure microwave plasma fluidized bed CVD of AlN coatings," Surface and Coatings Technology, vol. 203, no. 20–21. pp. 3168–3172, 2009.

[49].M. Tsukada, K. Goto, R. H. Yamamoto, and M. Horio, "Metal powder granulation in a plasma-spouted/fluidized bed," Powder Technology, vol. 82, no. 3. pp. 347–353, 1995.

[50].Lee and H. Sekiguchi, "Plasma-catalytic hybrid system using spouted bed with a gliding arc

discharge: CH$_4$ reforming as a model reaction," J. Phys. D. Appl. Phys., vol. 44, no. 27, 2011.

[51].Sanchez, G. Flamant, D. Gauthier, R. Flamand, J. M. Badie, and G. Mazza, "Plasma-enhanced chemical vapor deposition of nitrides on fluidized particles," Powder Technol., vol. 120, no. 1–2, pp. 134–140, 2001.

2. Experiments and data analysis

Here, we deal with the experimental set-up and the analysis methods we used in this project. Spouted bed experimental set-up, the plasma generator, and the particles used in the project will be included in the experiment procedure part. Apart from this procedure, the analysis methods will be summarized here which will also be described in detail in the following sections.

2.1 Experiment procedure

2.1.1 Spouted bed experiment set-up

A lab-scale plasma-enhanced spouted bed was created to study the behavior of the fine-particle fluidization process. Two kinds of spouted beds were made by quartz material, as shown in Fig 2.1.
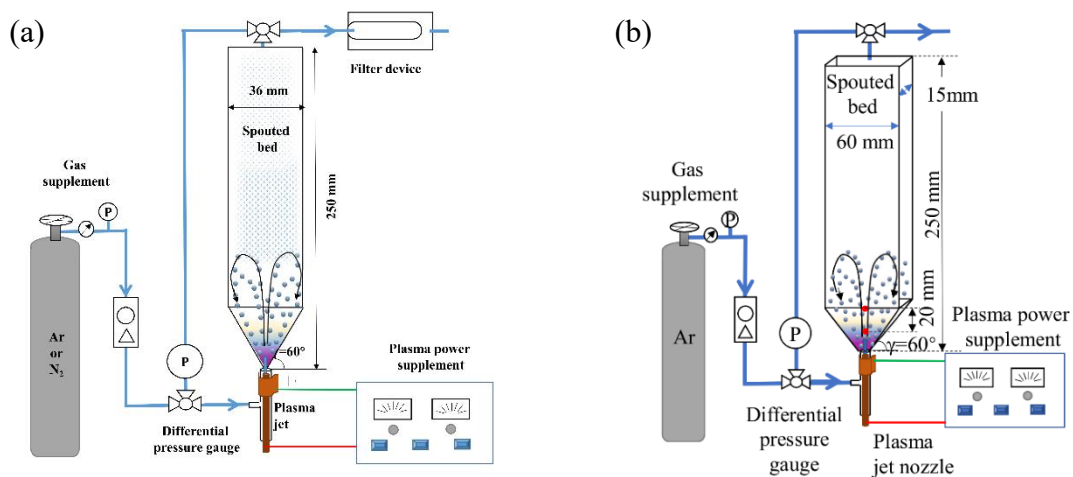

Fig 2.1 Schematic diagram of plasma-enhanced spouted-bed reactor unit

3D spouted bed and (b) 2D spouted bed

The three-dimensional (3D) quartz tube was presented in Fig 2.1 (a) (250 mm in height and 36 mm internal diameter) with an inlet angle of 60° (12.6-mm inner diameter). 2D spouted bed

was given here to analyze the plasma property, and the particle velocity profile easily. The two-dimensional (2D) spouted bed is made by quartz with the 60° inlet angle and 12.6 mm inlet diameter, as shown in Fig 2.1 (b). The height, width, and thickness of the spouted bed are 250 mm, 60 mm, and 15 mm, respectively.

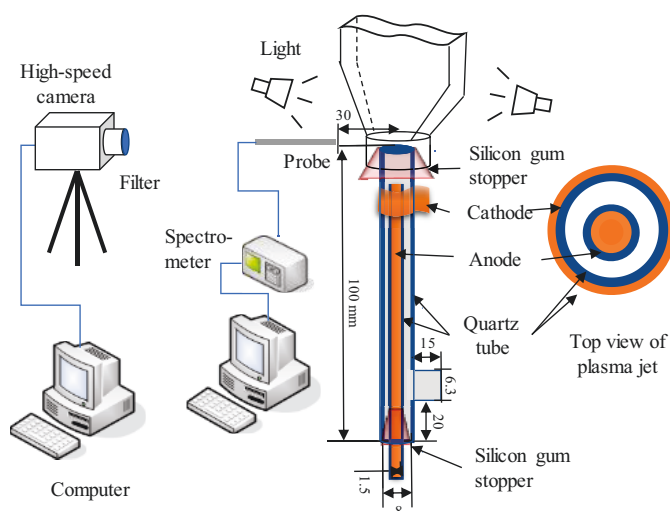### 2.1.2 DBD plasma jet generator

Fig 2.2 Plasma jet nozzle and the location of the spectrometer and high-speed camera

The plasma jet was a quartz tube (6-mm inner diameter and 100 mm in height) and was situated at the bottom of a spouted bed and connected to a silicone gum stopper as shown in Fig 2.2. A distributor with evenly distributed holes (0.5 mm diameter) was located at the top of the plasma jet tube to keep the fine particles stable. Here, the anode was a copper rod (1.5 mm diameter) inserted into an inner quartz tube as the dielectric barrier (1.5 mm internal diameter and 0.6 mm thickness) inside the plasma jet, while the cathode was a sheet of copper (20 mm length) covered on the outer quartz tube (7.2 mm external diameter) of the plasma jet.

The DBD-type plasma generator (PHF-2K-2U, Haiden Laboratory) with alternating current (AC) provided the plasma supply system. High-frequency power was supplied with a voltage

regulated in the range 0–10 kV and frequency in the range 0–100 kHz. DBD plasma was operated at a low frequency with 20 kHz in this research. The plasma gas was introduced from the side near the bottom of the plasma jet.

2.1.3 Materials

The average diameter of White fused alumina (WA) particles as the fine particles in this research were 58.6 μm, and the particle density was 1692 kg/m^3. Three kinds of large particles, polypropylene (PP) particle, black PP(BPP) and polyamide (PA) particle were adopted as the fluidized agents in our research (as shown in Table 2.1). BPP particle was covered by the black paint, which contains the primary material of acrylic resin and carbon, with a tiny layer on the surface. Average diameters of particles were the same of 3 mm, and average densities of particles are 897 kg/m^3, 910 kg/m^3 and 1140 kg/m^3, respectively.

Table 2.1　Fluidized agents

Particle	Abbreviation	Diameter	Density [kg/m^3]
White fused alumina particle	WA particle	58.6 μm	1692
Polypropylene	PP particle	3 mm	897
Black-Polypropylene	BPP particle	3 mm	900
Polyamide	PA particle	3 mm	1140

2.2 Analysis

2.2.1 Pressure drop

A differential pressure gauge was used to measure pressure fluctuation inside of the spouted bed. The pressure drop ($\triangle P$) of particles was calculated from the $\triangle P$ of spouted bed with the

addition of particles minus the $\triangle P$ of spouted bed. Future, the u_{ms} was calculated by the evolution of $\triangle P$ varied with gas velocity.

2.2.2 Void fraction

A laser sensor (Sensor head: IL-300, Amplifier unit: IL-1000, KEYENCE) was used for detecting the movement of the bed surface. Through the integral calculation of the changes of bed height ($\triangle H$), the expansion volume was calculated, which was usually presented by the changes of the void fraction (φ)

2.2.3 Optical emission spectroscopy

Optical emission spectroscopy (OES) was measured by a spectrometer (FLAME-S, Ocean Optics) and an optical fiber (P600-1-SR, Ocean Optics) with a wavelength of 200 to 886 nm (location is shown in Fig 2.2) with an integration time of 1 s. The detected points for OES data were noted as (x, y) = (0 cm, 0 cm) and (x, y) = (0 cm, 2 cm), which were showed by red circles in Fig 2.1 (b). While, the point of (x, y) = (0 cm, 0 cm) was the original point for the spouted bed, which was just above the plasma jet nozzle. The point of (x, y) = (0 cm, 2 cm) was equal to the initial bed height of 300 particles.

2.2.4 Plasma electron temperature

Due to the collision of particles in the plasma reaction process, the electron temperature (T_e), as one of the plasma parameters, should be calculated to characterize plasma. If we assumed the plasma is in a local thermodynamic equilibrium condition, the electron temperature could be calculated according to the emission intensity by the Boltzmann plot method. More details on the method by analyzing the emission intensity of Ar plasma-activated transmission can be found

in the last part. The plasma electron temperature in this thesis was analyzed by Boltzmann's plot of the Ar line spectrum at 357.215, 379.94, 706.7, and 800.616 nm.

2.2.5 Velocity profile analysis

The motion of particles in the plasma-enhanced spouted bed was taken by a high-speed camera (FASTCAM MiniAX100, Photron). The imaging system was controlled through the software of FASTCAM Viewer 3 (Photron). The particle velocity profile data is calculated by analyzing the average data from 1000 images with a duration time of 1 s, and the interval grid is 2 × 2 mm.

2.2.6 Other analysis

The temperature(T) of the spouted bed was measured by an infrared camera (FLIR T440, CHINO). A scanning electron microscopy (SEM) (JCM-6000Plus, JEOL Ltd.) was used to observe the surface morphology changes with plasma irradiation.

2.3 Summary

This chapter gives the details of the experimental set-up of the spouted bed and DBD plasma actuator. It is briefly introducing the experimental techniques including pressure drop of solid particle bed, optical emission spectroscopy of active plasma states, PIV and PTV measurement for the velocity file, spouted bed surface temperature and surface feature of particles.

3. Effect of plasma irradiation on the fluidization behavior for fine particles

3.1 Background

In the industrial chemical processes, systems combined with plasma have been studied for several years, but most are limited to the fundamental research and application process in fluidized beds. Fine particles, as the main agents in the industrial process, are challenging to fluidize and easy to lead the channel flow in the fluidization process. In this kind of system, the fluidization behavior of fine particles always is evaluated by the pressure drop ($\triangle P$) of particles and the minimum spouted velocity (u_{ms}). In the reports of Matsukata[1] Sathiyamoorthy[2] and Karches et al.[3], minimum fluidization velocity (u_{mf}) of fine particles have been decreased in the fluidized bed with various type of plasma generators. However, there is no report related to the fundamental fluidization behavior of the plasma-enhanced spouted bed process in literature, which is the dominant factor.

3.2 Experiments and conditions

In this chapter, a 3D spouted bed reactor combined with a DBD plasma generator at a low frequency (20 kHz) alternating current electric source was used to explore the effect of plasma irradiation on fluidization behavior. White fused alumina (WA) particles were used as the fluidized agent, which is a kind of typical particles in the field of ceramics, medicines, electronics, and machining processes. The average diameter of WA particles in this research was 58.6 μm, and the particle density was 1692 kg/m^3. The effects of particle volume, applied voltage, and

working gases on the behavior of fine particles were investigated in the experiments. The static

bed height (12–50 mm), gas velocity (0–1 m/s), applied voltage (0–9 V), and working gases (Ar

or N_2) were varied as shown in Table 3.1. The pressure drop and void fraction of the solid bed

were measured, and minimum spouted velocity (u_{ms}) was calculated to understand the

fluidization behavior of fine particles.

Table 3.1 Research process conditions

Category	Symbol	Unit	Variables
Static bed height of WA particles	H_0	mm	12 –50
Applied voltage	U	kV	0 - 9
Frequency	f	kHz	20
Working gas	-	-	Ar or N_2
Gas velocity	u	m/s	0 - 1

3.3 Results and discussion

3.3.1 Variation of pressure drop and u_{ms} in plasma-enhanced spouted bed

The dependencies of the bed pressure drop ($\triangle P$) of WA particles as a function of Ar gas

velocity (u) versus various static bed heights (H_0) without plasma enhancement are depicted in

Fig 3.1. A similar general trend occurred in these curves with four typical phases. $\triangle P$ increased

with the improvement of u from point A to B, and the solid bed remained as a fixed bed without

precise movement in the initial period. A hollow space and internal fountain appeared in the

bottom of the solid bed by increasing u continuously, which led to the $\triangle P$ continuously rising

until it reached a maximum value ($\triangle P_{max}$). The stage from A to B depended on the initial amount

of WA particles, which was longer with a high H_0 to overcome the resistance. $\triangle P$ declined along

BC because the height of the internal fountain became higher than that at the initial stage. As

point C approached, a noticeable expansion of the solid bed was observed by sufficient solid

movement in the top part of the solid bed. When u was increased beyond point C, the solid bed

surface was broken by the internal fountain. Point D represents the initial spouting position with

the u_{ms}[4]. $\triangle P$ decreased sharply as the concentration of the top fountain declined. With further

increases in u beyond point D, the spout region was stable regardless of the amount of gas and

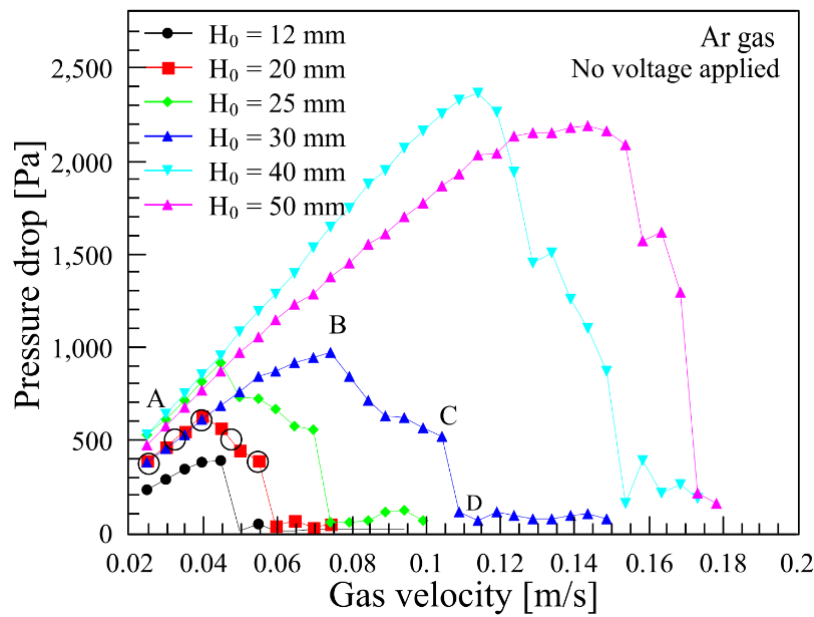increased the head height of the fountain without changes in $\triangle P$ naturally.

Fig 3.1 Variation of pressure drop with Ar gas velocity for different static bed height

without plasma (D point: minimum spouted bed velocity)

In the process of fluidization in the spouted bed, u_{ms} is a vital evaluation index to evaluate the

behavior of fine particles and is related to the column diameter (diameter of reactor (D_c) and inlet

spout diameter (D_i)), bed depth (H), and the physical properties of fine particles and gas (density

of solid and gas (ρ_s and ρ_g) and diameter of particles (d_p)) investigated by Mathur and Gishler[5]

as shown in Eq. (3-1).

$$u_{ms} = (d_p/D_c)\,(D_i/D_c)^{1/3}\,(2gH\,(\rho_s - \rho_g)\,/\rho_g)^{1/2} \tag{3-1}$$

To investigate the effect of plasma irradiation on the behavior of fine particles in a spouted bed, the applied voltages were changed from 0 kV to 7 kV for this system. Fig 3.2 compares the pressure drop versus gas velocity with different applied voltages with an initial bed height of 40 mm. The pressure drop decreased slightly in the curves from 0 kV to 5 kV. When the applied voltage changed to 7 kV, the pressure of the solid bed was much lower than that of the other conditions and was accompanied by a small u_{ms} value. It was found that the stage from point B to D was relatively shorter with a voltage applied than without voltage enhancement.
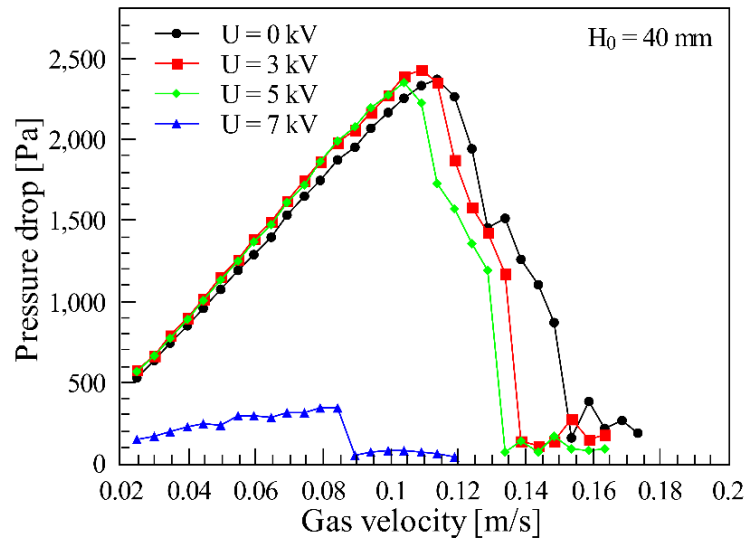

Fig 3.2 Variation of pressure drop with Ar gas velocity for various applied voltages

To gain more insight into the behavioral changes with applied voltage, Fig 3.3 shows the comparison results of $\triangle P_{max}$ and u_{ms} with several static bed heights under various applied voltages. There was a similar trend for $\triangle P_{max}$ and u_{ms} versus H_0 under low applied voltages (0 kV to 5 kV). In the presence of plasma, the $\triangle P_{max}$ and u_{ms} increased with an increase in the static bed height, which is consistent with the trend of an absent case. The $\triangle P_{max}$ and u_{ms} decreased

when 7 kV was applied regardless of the primary particle height. It must be mentioned that the direction of $\triangle P_{max}$ versus H_0 was different from that of u_{ms} with 7 kV applied. u_{ms} increased with the H_0 even when 7 kV was applied; however, the $\triangle P_{max}$ did not.
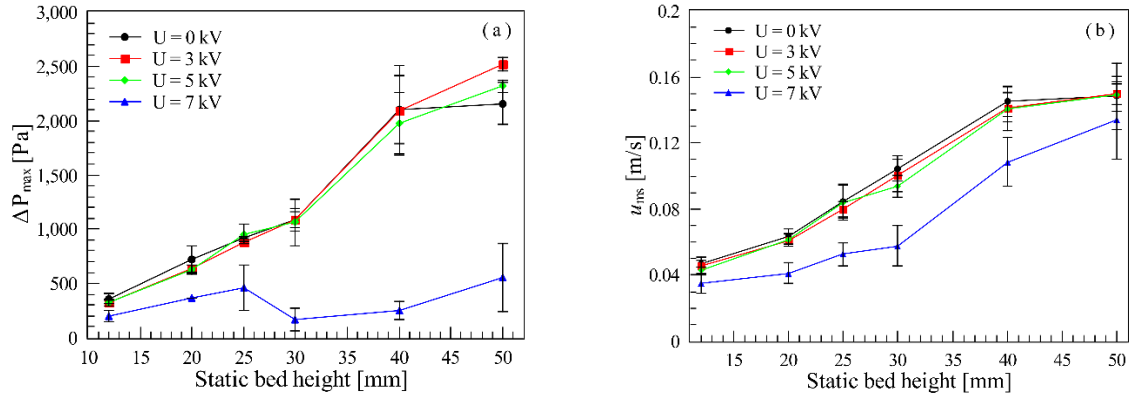

Fig 3.3 Variation of (a) maximin pressure drop ($\triangle P_{max}$) and (b) minimum spouted velocity (u_{ms}) with static bed height for various applied voltages

The trend for variation of $\triangle P_{max}$ and u_{ms} with the augmentation of H_0 under a low applied voltage was mainly related to the gravity of the solid bed. A higher H_0 with higher gravity and resistance impeded the gas from breaking through the solid phase. Under a low applied voltage, energy is not enough for gas ionization, and no changes occurred under 0 kV and a low applied voltage. On the contrary, under 7 kV, there was a significant decline in the $\triangle P_{max}$ and $u_{ms,}$ which may have been caused by the high ionization for the changes in the interaction between particles. In this study, the u_{ms} decreased by the plasma irradiation of gas, which is supported by the research of Sathiyamoorthy [2]. Therefore, high ionization gas easily forms a channel inside the WA particles. However, a small internal fountain with surrounding particles was not similar to the changes of u_{ms} because the $\triangle P_{max}$ did not change versus H_0.
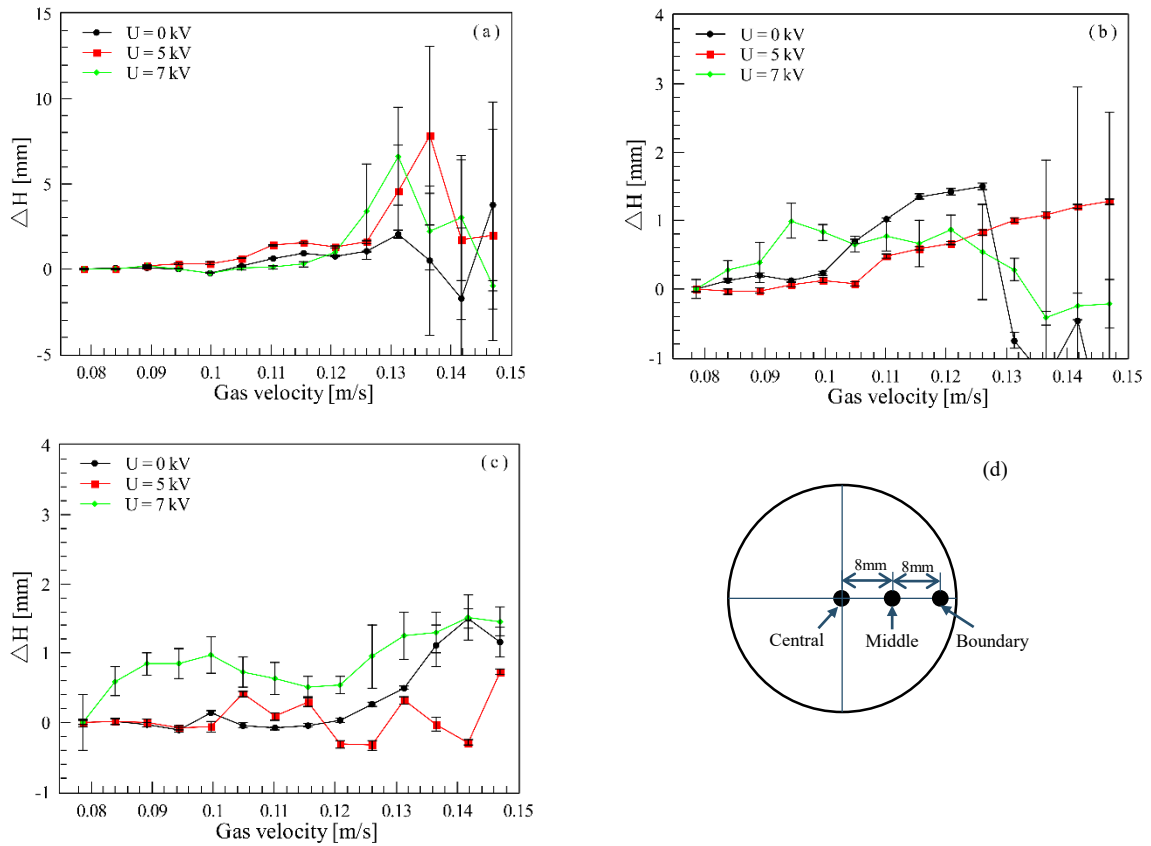
3.3.2 Effect of plasma irradiation on void fraction

Fig 3.4 Bed height changes versus gas velocity of Ar gas (H0 = 40 mm):

(a) central point, (b) middle point, and (c) boundary point, and (d) points location

To trace the reason for the u_{ms} changes, first, we want to confirm whether an interaction exists

between particles. However, the detection of interaction between particles is difficult, mainly

when voltage is applied in the process. Therefore, we measured the surface movement with a

laser sensor (IL-Intelligent) to detect the expansion of the solid bed while the velocity increased

with and without applied voltage. The detecting points were chosen, as shown in Fig 3.4 (d)

showing the top view of the spouted bed. Fig 3.4 (a) to (c) illustrate the height changes of the

solid particles ($\triangle H$) versus the gas velocity in different parts of the solid surface (central, middle,

and boundary points). Results show that $\triangle H$ increased with gas velocity regardless of the applied

plasma. The error bar of $\triangle H$ increased significantly when u passed the u_{ms} point (spouted fluidization situation), which means that the solid bed was experiencing severe vibration. Through the enlarged drawing of the section where u was less than u_{ms}, we can gain a better understanding of $\triangle H$ changes before the spouted point. The trend for the evolution of $\triangle H$ in the central section was similar to three applied voltages. In contrast, $\triangle H$ was much higher with 7 kV than the other conditions in the middle and boundary points, especially at the boundary point.

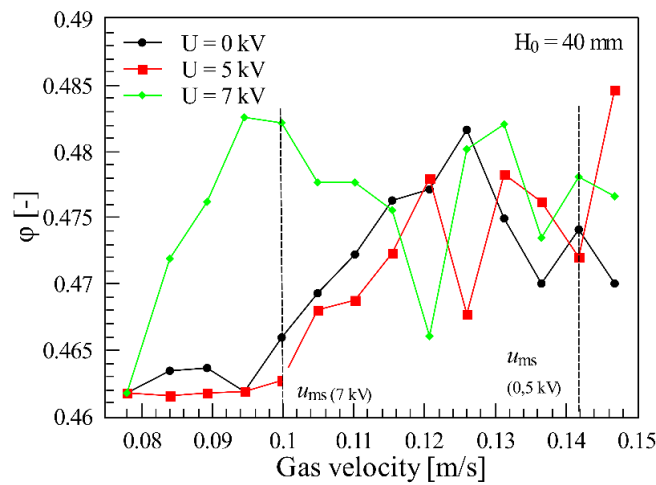Fig 3.5 Solid bed void fraction vs. gas velocity with different plasma voltage

Through the integral calculation of the changes of $\triangle H$, the expansion volume was calculated, which was usually presented by the changes of the void fraction (φ) as shown in Fig 3.5. Fig 3.5 gives priority to the differences of the void fraction before the spouted point of the solid bed. Similar changes of φ were found for the void fraction under 0 kV and 5 kV applied before u_{ms}. It is worth noting that the void fraction under 7 kV was more substantial than that of other applied voltages with low gas velocity. Even under a lower velocity, the solid bed expanded intensely with 7 kV applied compared to cases with lower applied voltage, which resulted in the void fraction increasing naturally. After the spouted point, the void fraction varied randomly

regardless of the amount of applied voltage. Combined with the inverse relation between φ and $\triangle P_{max}$, we can state that the decrease of $\triangle P_{max}$ resulted from the expansion of the solid bed.

Overall, the entire solid bed was shaken vigorously when 7 kV plasma was applied; however, in the absence of voltage, only the central part was shaken. It means that the solid bed under high voltage was not stable and led to a decreased interaction between the gas and solid particles and hampered the spouting of the solid bed (decline in u_{ms}). Matsukata [1] reasoned that the drop of u_{mf} was caused by the different dielectric loss and particle diameter characteristics and proved that the void fraction among particles is significant in the generation of plasma determination.

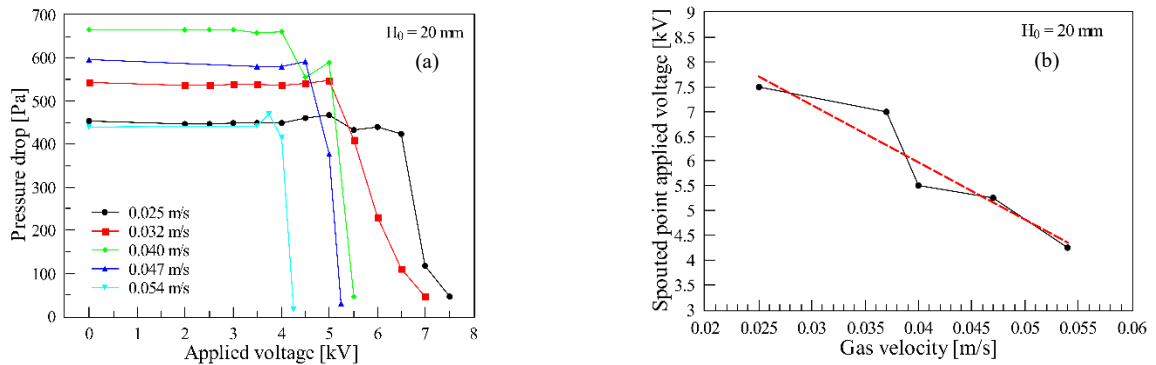### 3.3.3 Effect of applied voltages on fluidization behavior

Fig 3.6 (a) Pressure drop vs. applied voltage with different initial flow rates

(fixed flow rate (u₀) → fixed pressure drop (P₀) →

change the applied voltage (voltage maintained for 120s)), and

(b)   Relationship between spouted point applied voltage and gas velocity

To trace the reason for the decline of u_{ms} and eliminate the influence of flow rate, the effect of applied voltage on the particle fluidization behavior is considered in this section, especially for the remaining particles in a fixed bed situation. Five initial gas velocities(u_0) shown in Fig 3.1 were chosen with the condition of H₀ equal to 20 mm. Note that u_0 does not depend linearly

on the initial pressure (P_0) of these five points for investigating the primary influencing factor of u_0 and P_0. Once the u_0 was fixed, the applied voltage was changed from 2 kV to 7 kV with a maximum step of 0.5 kV for 120 s while recording the changes of pressure

Fig 3.6 (a) illustrates the pressure value of the solid bed versus applied voltage for 120 s treated at different gas velocities. The results show that the five curves with the same trend can be divided into two stages: a steady and slowly decreasing stage, and a sharply decreasing stage for changes in pressure. The pressure of the solid bed was kept stable as the applied voltage increased; once the voltage achieved a particular value, the pressure decreased to a small value; meanwhile, the solid bed turned into a spouted bed at the drop point. Comparing the different gas velocities, it was noted that the applied voltage value with a sharp descent of pressure was in accordance with the velocity and not with the initial pressure drop, which is summarized in Fig 3.6 (b). It is expected that particles also can be spouted in this system with the low gas velocity with the application of a high voltage.
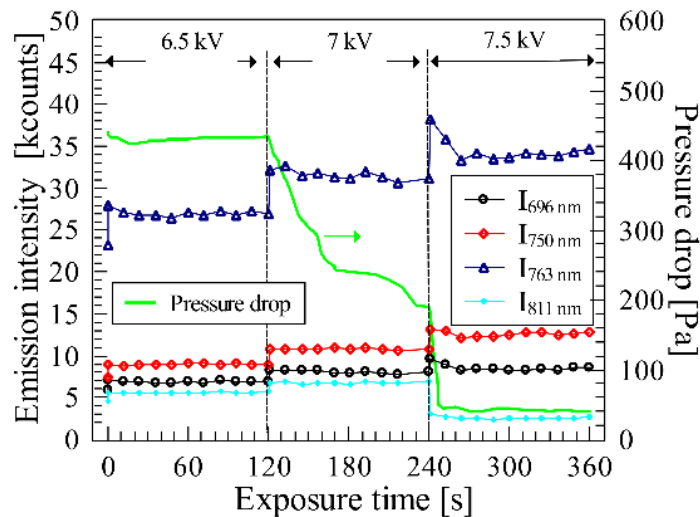

Fig 3.7 Evolution of the intensity of Ar bands and pressure drop of solid as a function of exposure time from 6.5 kV to 7.5 kV (H_0 = 20 mm, u = 0.025 m/s)

To investigate the changes in the gas phase when high voltages were applied, based on the evolution of the pressure drop shown in Fig 3.7, we measured the OES data for Ar plasma with an applied voltage to determine the relationship between OES changes and pressure drop in the solid bed. Emission intensity was the qualitative indicator of neutral unique number density[6] and was measured as OES data. Among the species, the transmissions of Ar (4p → 4s) are shown for a wavelength range of 695 to 840 nm. It is worthwhile mentioning that the peaks with wavelengths of 696 nm ($2p_2 \rightarrow 1s_5$), 750 nm ($2p_1 \rightarrow 1s_2$), 763 nm ($2p_6 \rightarrow 1s_5$), and 811 nm ($2_9 \rightarrow 1s_5$) are the characteristic peaks of Ar plasma gas. Fig 3.7 compares the pressure drop and the emission intensity in four peaks as a function of exposure time with a gas velocity of 0.025 m/s. Results reveal that when a high voltage was applied, the emission intensity for four bands increased suddenly and $\triangle P$ decreased. However, the increase in the emission intensity of the four bands was smaller at low voltages than that at high voltages, and $\triangle P$ remained relatively stable. In the high-voltage case, as time progressed, the emission of Ar lines at 696, 750, and 801 nm decreased at almost the same rate; however, the emission at 763 nm decreased at a much faster rate. The emission of Ar lines are identified with the evolution of $\triangle P$. A low voltage cannot supply enough energy for the sufficient ionization of Ar gas; nevertheless, the ionization of Ar gas increased once a high voltage was applied. More ions and electrons were produced among the solid bed because of the high ionization of Ar gas, resulting in an increase of space among particles and eventually leading to a significant decline in the pressure drop. With the decline of $\triangle P$, the solid bed expanded, which decreased the emission intensity for the Ar bands but was still higher than that with a low applied voltage. It can be inferred that ionization may be the

central point for the $\triangle P$ decline of a plasma-enhanced solid in a spouted bed process.

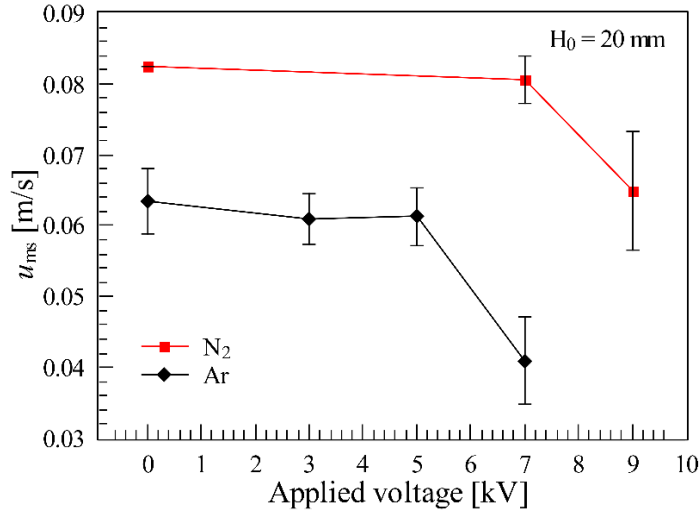### 3.3.4 Effect of working gas on fluidization behavior

Fig 3.8 Minimum spouted velocity vs. plasma voltage for Ar and N_2 gas

To further confirm that ionization is the main reason for particle behavior changes, two working gases with different degrees of ionization, Ar and N_2, were investigated in the process of fine particle behavior in a spouted bed. The relationships between u_{ms} and applied voltage with Ar and N_2 gas are illustrated in Fig 3.8. A specific value of applied voltage was supplied before the experiment with a small amount of gas. The gas velocity was increased slowly to determine the u_{ms} point. Fig 3.8 shows that the u_{ms} with N_2 was higher than that of Ar without an applied voltage, which is contributed to the difference in density, 1.613 kg/m^3 for Ar gas and 1.13 kg/m^3 for N_2 gas. Also, u_{ms} declined as the applied voltage increased when the voltage was higher than 7 kV. At 7kV applied voltage, the decreasing amplitude of Ar was much larger than that of N_2 because of the difference in gas breakdown voltages. In Matsukata's[1] research, alumina particles were fluidized in Ar and H_2 with a 200 W microwave plasma system. Results showed that the u_{mf} decreased with an Ar plasmatic condition; however, it was identical in the H_2 plasma

system. The reason for this phenomenon might be attributed to the difference of the $(e_r)^{-1}$ values

for H_2 (253.8×10^{-6}) and Ar (517.2×10^{-6}). In our case, by visual observations, stable N_2 plasma

was more difficult to generate in the spouted bed than Ar. Furthermore, the $(e_r)^{-1}$ value for N_2

(470.6×10^{-6}) is smaller than that of Ar, which means with 7kV plasma applied, the ionization of
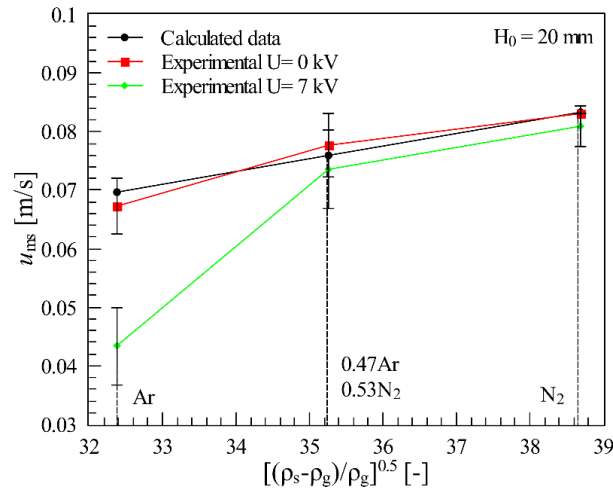
N_2 is much less than that of Ar.

Fig 3.9 Minimum spouted velocity vs. density of gas and particles

Based on this, we compared the results of u_{ms} of the calculated data based on Eq. (3-1) and

the experimental data with applied voltages of 0 kV and 7 kV in the conditions of Ar, N_2, and a

mixture of the two, as shown in Fig 3.9. Results show that the u_{ms} data with the absence of plasma

were in accordance with the calculated data from Eq. (3-1). However, with the presence of

plasma under 7 kV, a linear relationship did not occur between the u_{ms} and the x-axis. The

electrons of the gas increased by the ionization of the gas, which increased the pressure of the

gas and the volume of discharged gas. It can be proved that the gas density of the discharge gas

should decrease, which is the opposite conclusion of the data calculated from Eq. (3-1). It may

be because of Eq. (3-1) of u_{ms} is not suitable in the plasmatic condition, and the presence of N_2
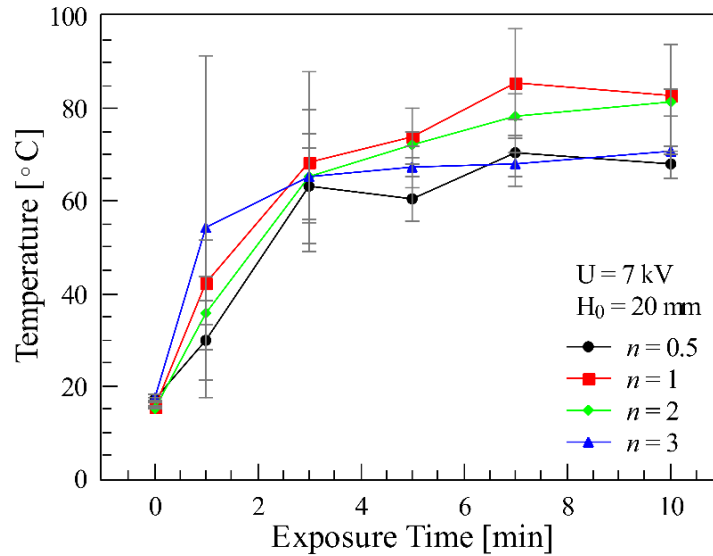
restrained the ionization degree of Ar.

Fig 3.10 Surface temperature of the inlet point of the spouted bed

The temperature changes were measured for the spouted bed. It was difficult to detect the bed temperature because of the thermocouples effected by the ionization of the gas. Therefore, the inlet of the spouted bed was chosen to measure the temperature by an infrared camera (FLIR T440). The inlet-point temperature was equal to the inside temperature after a long time detected by a thermocouple. Fig 3.10 illustrates the inlet temperature changes versus various velocity conditions of Ar. The ratio of u to u_{ms} was equal to n. There was no significant difference for inlet points after 5 min. Based on the temperature changes, the volume of gas can be increased by approximately 7% in theory, which leads to changes in gas density insufficient enough to significantly decrease u_{ms}. It is not consistent with Eq. (1), which means u_{ms} will increase while the gas density decreases not only by an increase in temperature but also by the ionization of the gas.

Typical SEM micrographs of the primary WA particles and the WA particles treated with the

7 kV enhanced plasma with 1.0 m/s Ar gas velocity after 10 min are illustrated in Fig 3.11. There was no significant abrasion and surface damage after plasma enhancement even under high voltage. The shape of WA particles and the diameter did not significantly change, which excludes the effect on the particles' fluidization behavior changes.
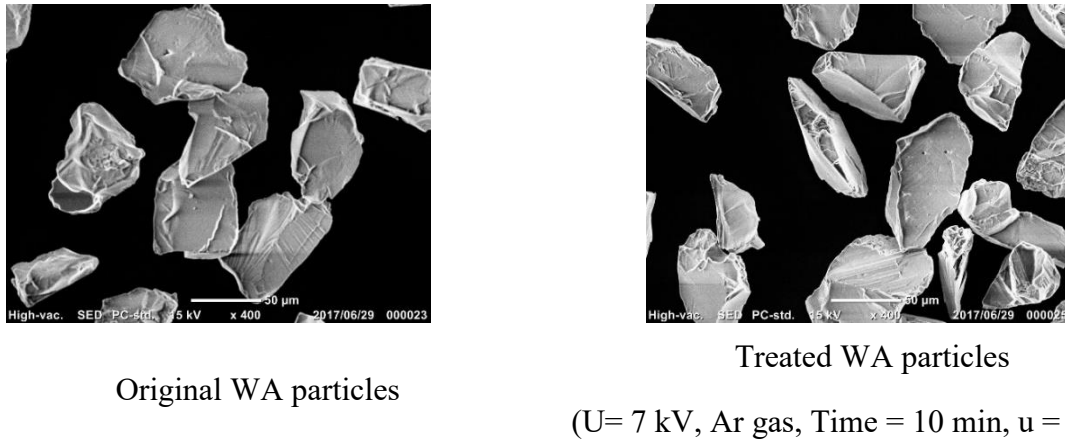

Original WA particles

Treated WA particles

(U= 7 kV, Ar gas, Time = 10 min, u = 1.0 m/s)

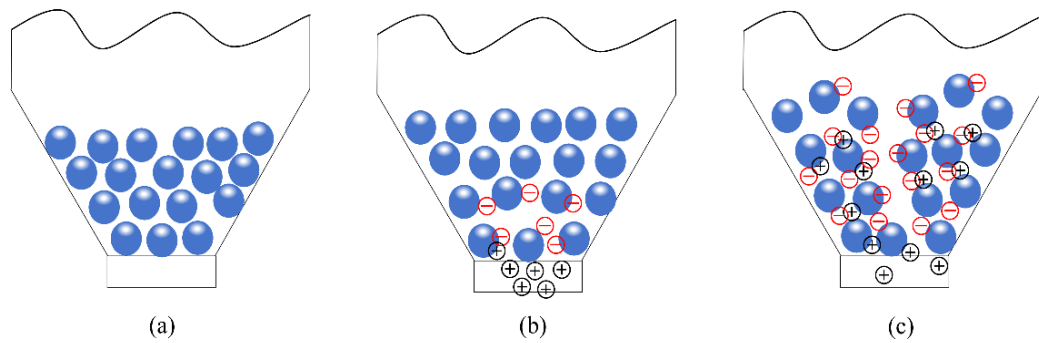Fig 3.11 SEM images of WA particles

(a)　　　　　　　　(b)　　　　　　　　(c)

Fig 3.12 Mechanism for particle charged in plasma-enhanced spouted bed:
(a)   fixed bed with gas insulation phase, (b) expansion situation with gas discharge phase, and (c) spouted bed with gas breakdown phase.

To summarize, we illustrated the image of the mechanism for charged particles in the plasma-enhanced spouted bed in Fig 3.12. Before the spouted situation, the solid bed can be divided into three phases: (a) fixed bed with gas insulation phase, (b) expansion situation with gas discharge phase, and (c) spouted bed with gas breakdown phase. In the stable stage shown in Fig 3.12 (a),

a small amount of ionization with free diffusion among the gas occurred with a low applied voltage or a small amount of gas velocity. The small quantity of ionization was insufficient to change the gas into plasma, and constant pressure was maintained. With an increase in the applied voltage or the amount of gas, the number of electrons increased slightly, as shown in Fig 3.12 (b). The electric field was not high enough to supply sufficient energy to cause an inelastic collision of gas. When the discharge of gas started, the electrons and ions of the gas phase, eventually led to the gas breakdown phase. A particle will be charged with an anion sooner than that of a positive electron because the velocity of the ion is higher than that of the electron. The repulsive force among the particles causes the particles to reject each other because of the small amount of power in the initial time and explains the increase in the void fraction in Fig 3.5. As the voltage or amount of gas increased continuously, the energy was sufficient by the continuous ions and electrons to overcome resistance among the particle bed, as shown in Fig 3.12 (c). The repulsive force was high enough to form a microchannel until the power increased to a particular value and made it possible for the gas to penetrate the spouted bed situation, and therefore, $\triangle P$ declined.

3.4 Summary

The combined system of DBD plasma with a spouted bed reactor was adopted in this chapter to determine the fluidization behavior of fine particles. The pressure drop, u_{ms}, void fraction were detected in the process with the plasma irradiation. The effect of plasma irradiation on the fixed bed and the effect of working gas on the fluidization behavior were researched.

Due to the inherent interparticle forces (triboelectrification and Van der Waals) and interparticle forces from the charge from plasma irradiation, especially by repulsive force form the charge on the surface of WA particles (insulated particles), the void fraction of solid bed was enhanced, which means the distance of particles improved. It resulted in the pressure drop of solid bed decreased and u_{ms} declined by the enhancement of applied voltage irrespective of the static bed height and type of working gas. The interaction among particles with 7 kV applied voltage resulted in the enrichment of the void fraction before fluidization started; moreover, the entire solid bed was expanded when a high voltage was applied. Even for a solid fixed bed with a low gas velocity, enhancing the applied voltage led to a change of solid bed from a stable manner to the spouted fluidization. Combined with the OES data, the emission intensity for Ar plasma species increased, and $\triangle P$ decreased with the enhancement of applied voltage. It is consistent with the mechanism that the ionization of the working gas was the main reason for the variation in particle fluidization behavior. It suggests that the plasma irradiation changed the fluidization behavior of solid bed, which can be used for the plasma process with the low-speed requirement. The next step is to focus on the movement of particles in the combination system to obtain further fluidization behavior changes.

3.5 References

[1].M. Matsukata, K. Suzuki, K. Ueyama, and T. Kojima, "Development of a microwave plasma-fluidized bed reactor for novel particle processing," Int. J. Multiph. Flow, vol. 20, no. 4, pp. 763–773, Sep. 1994.

[2].Sathiyamoorthy, "Plasma spouted/fluidized bed for materials processing," J. Phys. Conf. Ser., vol. 208, no. 1, p. 12120, Feb. 2010.

[3].M. Karches, C. Bayer, and P. Rudolf Von Rohr, "A circulating fluidised bed for plasma-enhanced chemical vapor deposition on powders at low temperatures," Surface and Coatings Technology, vol. 116–119. pp. 879–885, 1999.

[4].K. Mather, Spouted Beds. Elsevier Science, 1974.

[5].B. Mathur and P. E. Gishler, "A technique for contacting gases with coarse solid particles," AIChE J., vol. 1, no. 2, pp. 157–164, Jun. 1955.

[6].M. V. Malyshev and V. M. Donnelly, "Determination of electron temperatures in plasmas by multiple rare gas optical emission, and implications for advanced actinometry," J. Vac. Sci. Technol. A Vacuum, Surfaces, Film., vol. 15, no. 3, pp. 550–558, 1997

4. Optical emission spectroscopy diagnostics of DBD plasma with particles

4.1 Background

There are many unique types of research in the literature dealing with the basic concepts of detecting the characteristic of plasma. The photons caused by the electronically excited states of the plasma species in the transition processes are recorded with characteristic wavelengths[1]. Among the detecting techniques, optical emission spectroscopy (OES) is a conventional technique with high accuracy and no intrusiveness by recording the emission intensity of each wavelength. The emission intensity is the qualitative indicator of neutral unique number density[2]. In our previous research, it was also clarified that the fluidization behavior of fine particles was changed by the plasma irradiation in a spouted bed [3]. The minimum spouted velocity (u_{ms}) for fine particles was decreased, and the void fraction was enhanced with high applied voltage. It is well accepted that the positive effect of plasma irradiation on the particle fluidization behavior. However, no information has been done to analyze the characteristic of plasma with the presence of particles in a spouted bed. Hence, we herein investigate the role of particle fluidization behavior on the optical emission spectral characteristics of plasma in a DBD plasma-enhanced spouted bed.
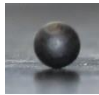
4.2 Experiments and conditions

This chapter proposes a combination of DBD plasma with a 2D spouted bed system with Ar gas as the plasma gas. The DBD plasma jet replaces the spouted bed jet, which is contributed to

the gas state changed to the plasma state. We aim to investigate the effect of particles fluidization behavior on the optical emission spectroscopy diagnostics of the DBD plasma in a spouted bed.

Two kinds of particles, polypropylene (PP) particle and black PP (BPP) particle were adopted as the fluidized agents in our research. BPP particle was covered by black paint, which contains the main material of acrylic resin and carbon, with a tiny layer on the surface. Average diameters of PP and BPP particles were the same of 3 mm, and average densities of particles are 897 kg/m^3 and 910 kg/m^3, respectively. The fluidization behavior for the two kind of particles almost the same due to the similar diameter and density. Different surface color related to the reflection and absorption of the plasma light. Applied voltage (0 kV to 7 kV) and flow rate (0 to 20 m/s), and the number of particles (0 to 500) were changed as illustrated in Table 4.1. The optical emission spectral characteristics and the effect of fluidization behavior on the emission intensity of Ar plasma were obtained.

Table 4.1 Research process conditions

Category	Symbol	Unit	Variables	
Particle type	–	–	PP particles	BPP particles
Particle number	–	–	0 – 500	
Applied voltage	U	kV	0 – 7	
Flow rate	u	m/s	0- 20	

4.3 Results and discussion

4.3.1 Fluidization behavior

To gain insight into the effect of particle fluidization behavior on the DBD plasma optical characteristic, it is essential to obtain the fluidization behavior of particles firstly. Fig 4.1 illustrates the typical results of pressure drop against gas velocity for 300 particles. The solid markers in Fig 4.1 refer without plasma irradiation, and the hollow markers refer with 7 kV voltage. The trend of the pressure drop for particles as the function of the Ar gas velocity was similar to those trend reported in the literature[4]. Since the particle size was large in this
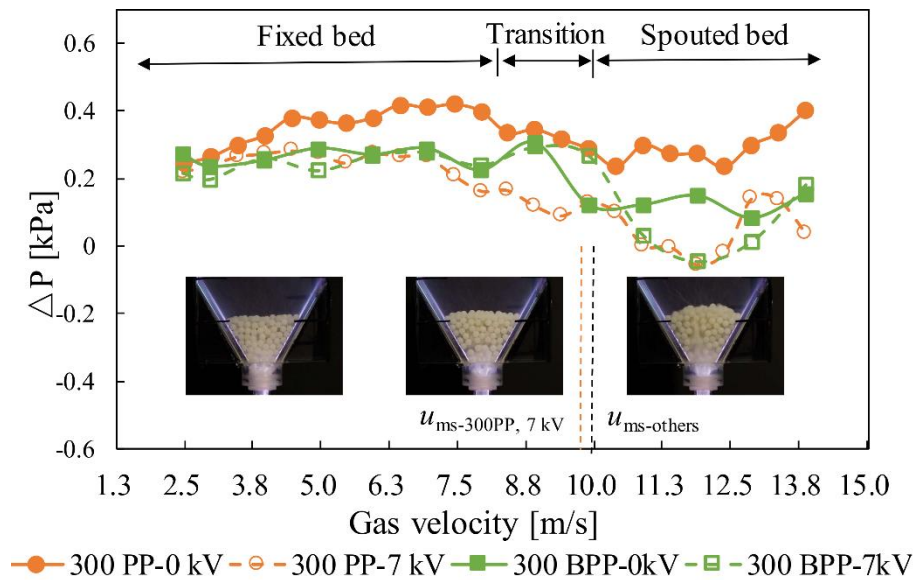

Fig 4.1 Variation of pressure drop with a gas velocity of Ar gas without 0 kV and 7 kV applied voltage, and digital imaging of fluidization pattern (applied voltage: 7 kV) (F value: 1.8, and exposure time: 0.08 s)

experiment, a significant difference in the pressure drop by the plasma irradiation was not observed as the data shown for fine particles in our previous chapter[3]. As can be seen, the pressure drop increased with an increase in gas velocity. Then, the pressure drop declined slightly

as the presence of a fountain in the spouted bed regardless of particle types. As the low gas velocity, the particles were still in the fixed bed satiation without movement both for PP and BPP particles. When the gas velocity increased around u_{ms}, particles started to fluidize, which means the particles moved as a fountain with a little space between each other. As the gas velocity increased more, the fluidization behavior was too intensive related to the large space between particles. There was a period for all particles moved as a fountain with a stable manner and a stable distance between each other at the gas velocity just above u_{ms}, which we called as good fluidization behavior period. Admitted of comparison with the digital images of the three phases for PP particles, the void fraction of solid bed enhanced obviously with high gas velocity. The void fraction for BPP particles was almost the same as the PP particles. The pressure drop was declined with 7 kV applied voltage in the case with PP particles, which means the u_{ms} decreased slightly.

The reason for the difference of pressure drop by applying voltage was researched in our previous paper[3] that the plasma irradiation effected on the charge on the particle surface. It is noteworthy that the fluidization behavior of BPP particles was not changed significantly by plasma irradiation. Due to the similar density for PP and BPP particles, the effect of density difference on the fluidization behavior can be ignored. Besides, the temperature of spouted bed at the detected point of (x, y) = (0 cm, 0 cm) was almost same (around 33°C) for two kinds of particles with the 7kV voltage applied at the gas velocity of u_{ms}. However, due to the BPP particles were covered with the carbon material with a thin layer, the surface material had been changed compared to the PP particles even with the same inside material. Based on the research

data[5] showed that the electrical conductivity of PP material mixed with carbon fillers enhanced than PP material. Due to the material determines the electrical conductivity, in our research, the electrical conductivity on the surface had been changed from insulative (PP particles) to conductive (BPP particles). Even though in Morooka's research [6], he mentioned that it was dominant of the influence of electrical conductivity of ultrafine powders ($CaCO_3$ and $CaCO_3$ blended with carbon black) on the fluidization quality. However, in the case of large particles, the interaction force between particles is not so much as between ultrafine powders. The effect of electrical conductivity for the large particles cannot be neglected due to the difference in the charge transfer rate. It can be assumed that the electron charge by gas discharge has been changed from the charge model (surface charge)[3] to the transfer model.
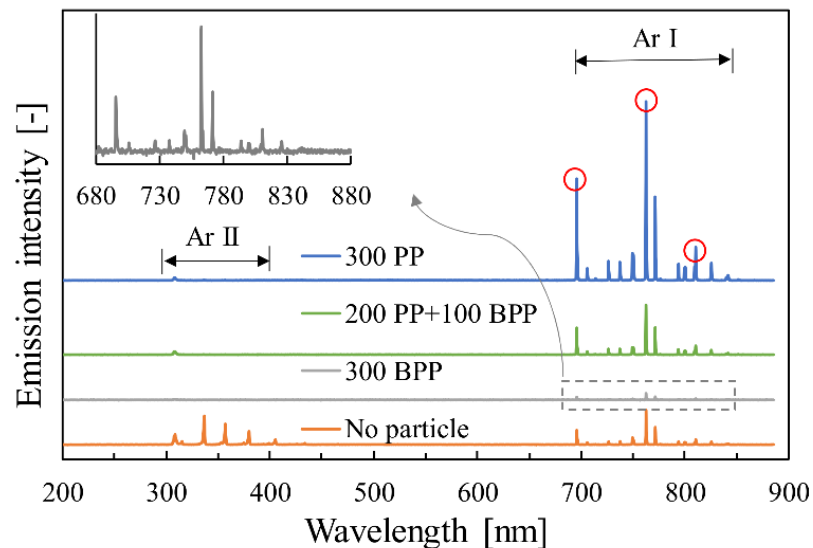
4.3.2 Optical emission spectral characteristics

Fig 4.2 Optical emission spectra of Ar plasma with 7 kV applied voltage

($u = 9.9$ m/s and detected at (x, y) = (0 cm, 0 cm) point)

To Figure out the effect of fluidization behavior on the plasma characteristic, we detected the optical emission spectra of plasma at the point of (x, y) = (0 cm, 0 cm) with particles in the

spouted bed. Fig 4.2 presents the spectral emission data of Ar plasma for various conditions with a gas velocity of 9.9 m/s (u_{ms} of 300 particles, where the particles began to be fluidized). The emission intensities with the quartz spouted bed and without quartz bed were almost the same so that in this chapter, the case of no particle was installed with the quartz spouted bed. Based on the atomic data from the NIST Atomic Spectra Database[7], the wavelength with a range of 300 to 410 nm belong to the transition lines of Ar II, and infrared spectrum (700 – 840 nm) was dominated by the atomic spectrum of Ar I transition lines. There was a significant difference in spectra by the presence of particles. In comparison with BPP particles and PP particles, the Ar II spectra were decreased obviously in both cases, and most of the wavelengths cannot be detected when the particles were added. That is, only the Ar I spectra changed (increased or decreased) significantly as the presence of particles. In the enlarge Figure of BPP particles, the detail emission intensity from 700 to 840 nm still presented even with low value. Nevertheless, significant enhancement of Ar I spectra part (5 times than no particle) was detected with PP particles. In the case of the mixture particles, the emission intensity with 67% PP particles in the mixture particles of PP and BPP was much lower than 100% PP particles.
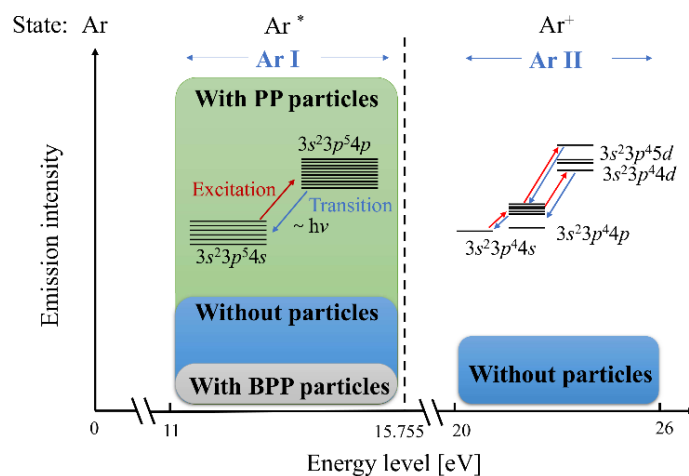

Fig 4.3 Partial energy-level diagram for Ar I and Ar II in this research

There are so many plasma-chemical reactions[8] considered in the numerical code. Between the ground state and excited Ar states, processes of elastic scatting, diffusion, excitation and transition have existed. As the partial energy levels suitable in our paper are shown in Fig 4.3, all the excited states are regarded as the numbers of levels. The color area presents the emission intensity for various situations. The excitation reactions are presented as the red lines, and transition reactions are showed as blue lines. In the case of without particles, Ar I and II transition lines can be observed (as the blue parts show). The emission intensity of Ar I transition lines were increased with PP particles (as the green part shows) and decreased with BPP particles (as the grey part shows). Due to the presence of an electric field and the collision between Ar gas atoms, there were some electrons already presented in Ar gas. The excitation and ionization processes were presented by the collisions between an electron and Ar atom, especially by the inelastic collision. The electrons in the Ar atom excited to the higher energy level by absorbing the energy from a high voltage applied.

However, the excited state for an atom was not stable, which results in transiting to the ground state again with the release of energy presented by light photons in visually. The light photons analyzed as the emission spectra of the plasma species as the spectral data shown in Fig 4.2. Based on the spectral data in our research, the species of Ar I($4s$), Ar I($4p$), Ar II($4s$), Ar II($4p$), Ar II($4d$), and Ar II($5d$) are involved in the kinetic model. However, transitions from Ar II $4s$ $\rightarrow 4p$, Ar II $4p \rightarrow 4d$, and Ar II $4p \rightarrow 5d$ have high energy levels, which means that the electron needs high energy for the collision to the Ar ion (Ar$^+$)states. Based on the data shown in Fig 4.2, most of Ar II lines cannot be detected by adding particles. Due to the energy between atom and

particles were conservative, the frequency of excitation processes and transition processes were increased by the increase of collision between atom, electron, and particles. It means that the most atomic Ar excited to the excited state (Ar*) state with the addition of particles. So, the probability of transitions for Ar II lines were decreased correspondingly. We can assume that the more generations of these active species for Ar I rely on the ability of the plasma to produce a high concentration of excited and ionized (active) plasma species.

However, it is essential to highlight that with the addition of BPP particles; the emission intensity data was the lowest in these three situations. We assumed that the reason for the difference for the plasma emission intensity with particles might be in connection with the particle types. There is no denying that the color of particle surface effects on the absorption and reflection of the light photon. Based on the results from ultraviolet-visible spectrophotometer (Jasco, V770) in a range of 200 to 1000 nm, the higher average reflection rate (highest value of 52%) and lower absorption rate (lowest value of 45%) can be found with PP particles than that of BPP particles (3% for reflection rate and 96% for absorption rate). The absorption by the black surface of BPP particles maybe results in the detected emission intensity decreased. In contrast, due to the white color of PP particles, the reflection of the surface may also enhance the detected numbers of the photon in the direction of optical fiber. However, refer to the discussion showed in Fig.4, we cannot say that the amount of electron and ion was decreased with BPP particles. So, the color of the particle surface related to the reflection and absorption influences on the detected emission intensity. It is also necessary to detect the emission intensity with particles for a broad wavelength included the infrared spectroscopy.

4.3.3 Effect of applied voltage on the plasma characteristics

(a)   Applied voltage: 3 kV   (b)   Applied voltage: 5 kV   (c)   Applied voltage: 7 kV
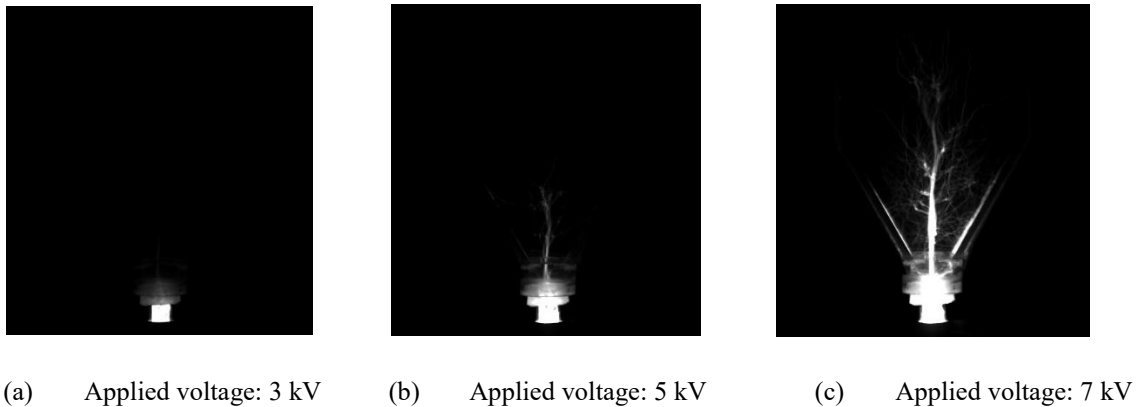
Fig 4.4 High-speed camera imaging of plasma with different applied voltage

(particle number : 0, gas velocity: 15.1 m/s, and frame rate: 750/s)

The applied voltage provides the electric field for generating the plasma. To achieve the effect of applied voltage on the optical emission spectral characteristics, Fig 4.4 (a) to (c) illustrate the images of plasma photon lines versus applied voltages token by a high-speed camera. With 3 kV applied voltage, we cannot observe so many plasma photon lines. With the increase of applied voltage, the amount and length of plasma lines were enhanced.

To figure out the enhancement of emission intensity with the increase of applied voltage, Fig 4.5 (a) and (b) show the relationship between the applied voltage and emission intensity without particles and with 300 PP particles at the detected point of (x, y) = (0 cm, 0 cm). In the full view, the emission intensity was increased with the applied voltages, which was corresponded well with the images showed in Fig 4.4. The highest value of emission intensity with 300 PP particles was five times than that of without particles. The emission intensity was low with 3 kV and 4 kV applied voltage regardless of particles. When the applied voltage increased over 5 kV, the emission intensity for Ar I spectra increased significantly in both cases. However, Ar II spectra

just increased in the case of without particle, but no noticeable changes can be observed with 300
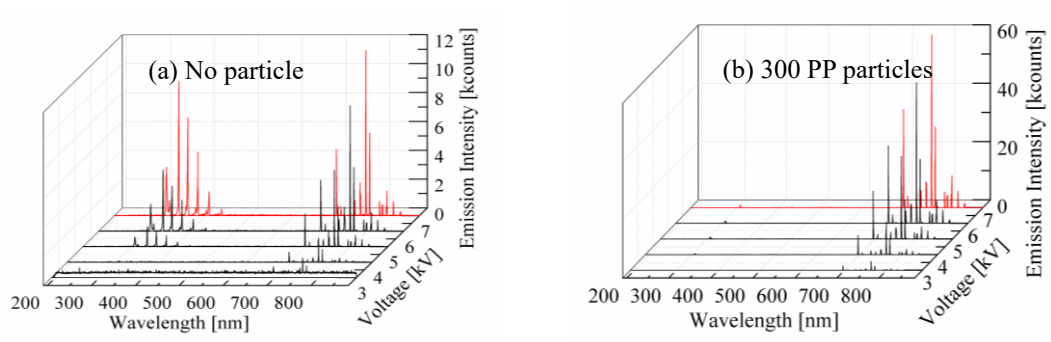
PP particles.

Fig 4.5 Variation of emission intensity with wavelength for various applied voltages

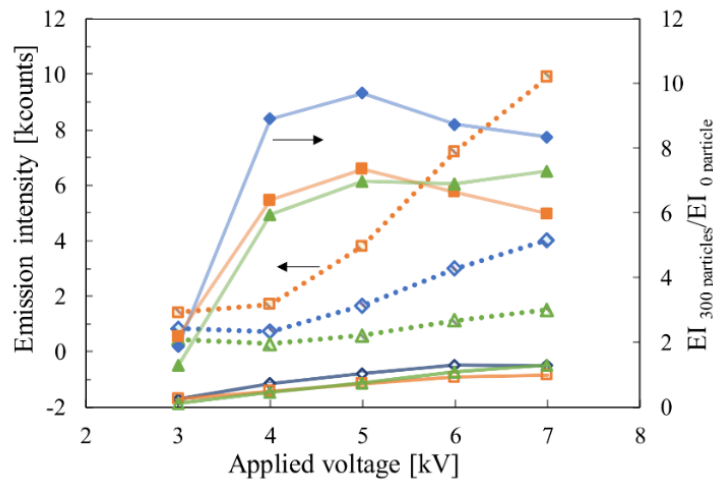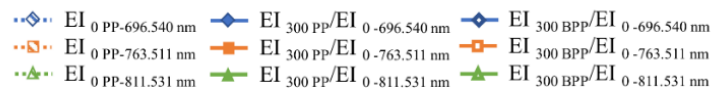(u = 9.9 m/s and detected at (x, y) = (0 cm, 0 cm) point)

Fig 4.6 Emission intensity vs. applied voltages for different wavelengths

(u = 9.9 m/s and detected at (x, y) = (0 cm, 0 cm) point)

To further confirm the relationship between applied voltage and emission intensity in detail,

Fig 4.6 presents the effect of applied voltage on the emission intensity. We selected three

wavelengths of 696.54 nm, 763.511 nm, and 811.531 nm to compare the details. Those

wavelengths were the characteristic peaks of Ar I plasma spectra as the circle points shown in

Fig 4.2. $EI_{300\ particles}$ refer to the emission intensity of plasma with 300 particles, and $EI_{0\ particle}$ refers to the emission intensity without the addition of particles. There was no noticeable change for the emission intensity with the voltage increased from 3 kV to 4 kV without particles as the dotted lines show. When the applied voltage increased over 4 kV, a linear relationship can be found between applied voltage and emission intensity for various wavelengths. In the presence of particles, the ratio of the emission intensity with particles to without particles ($EI_{300\ particles}/EI_{0\ particle}$) are illustrated by the solid markers (300 PP particles), and the hollow markers (300 BPP particles). $EI_{300\ particles}$ refer to the emission intensity of plasma with 300 particles, and $EI_{0\ particle}$ refers to the emission intensity without the addition of particles. It can be mentioned that the ratios of $EI_{300\ particles}/EI_{0\ particle}$ were entirely different for two kinds of particles. In the case of 300 BPP particles, the ratio increased by applied voltage slightly, but always around to 1. It means that the changes in emission intensity with 300 BPP particles almost similar to the absence of particles regardless of wavelengths. However, in the case of 300 PP particles, the ratio of $EI_{300\ PP\ particles}/EI_{0\ particle}$ increased to a high value from 4 kV, then presented almost a stable trend with the increase of applied voltages. It means that the slop of emission intensity to applied voltage with 300 PP particles is much higher (6 to 10 times) than that of no particles. We should notice that the ratio of $EI_{300\ PP\ particles}/EI_{0\ particle}$ was the difference for three wavelengths, especially for the wavelength of 696.54 nm. The electron excitation cross-section of different energy levels changed at different rates maybe give the reason for the difference in the increase rate of emission intensity for the excited spectral lines.

As the low voltage applied, the electron energy and the impact cross-section are relatively low, which result that the electron and Ar collision probability is not high enough[9]. As the high voltage applied, the degree of plasma ionization accrued, more electrons and excited states produced per time unit, which leads to the increase of emission intensity[10] as exhibited in Fig 4.5 and Fig 4.6. It is supported by Wei's research[11] that a high applied voltage would produce a high electron density and enhance the electric intensity sustained in the discharge region. With the addition of PP particles, the emission intensity increased significantly with a high applied voltage. Based on the mechanism showed in Fig. 4, it means that with the high applied voltage and with the PP particles, more concentration of excited and ionized (active) plasma species can be produced.

4.3.4 Effect of gas velocity on the plasma characteristics

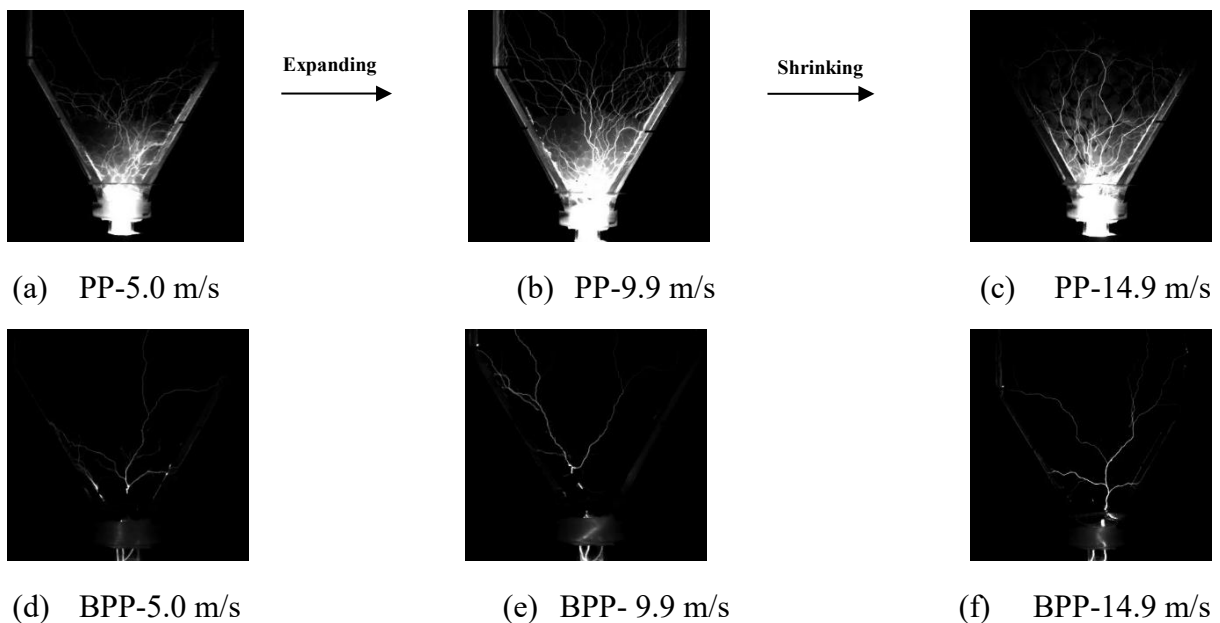| (a) PP-5.0 m/s | (b) PP-9.9 m/s | (c) PP-14.9 m/s |
| (d) BPP-5.0 m/s | (e) BPP- 9.9 m/s | (f) BPP-14.9 m/s |

Fig 4.7 High-speed camera imaging of fluidization with different gas velocity

(particle number : 300, applied voltage : 7 kV, and frame rate : 750/s)

To investigate the effect of gas velocity on the plasma emission intensity, we took several

images of plasma situation with 300 PP and BPP particles by the high-speed camera (illustrated in Fig 4.7). The difference for the plasma behavior can be well known primarily from PP images. With the increase of gas velocity from 5.0 m/s to 9.9 m/s, the brightness part in the spouted bed expanded. However, when the gas velocity increased to 14.9 m/s, the brightness region changed to shrink. However, we can not see much plasma lights in the images for BPP particles various gas velocities.
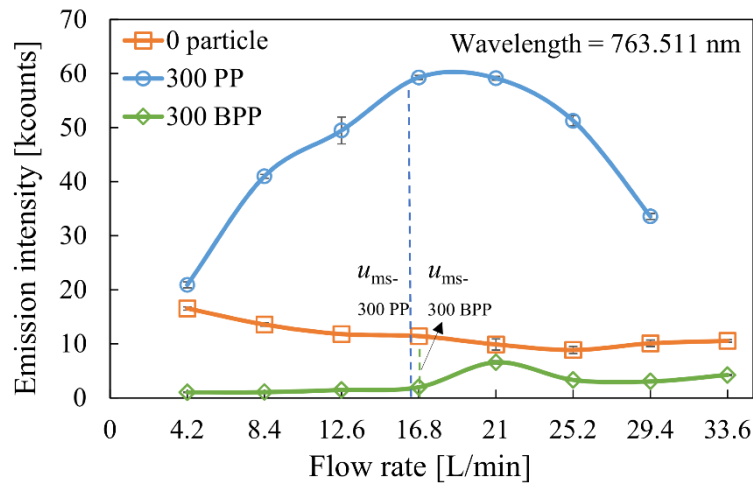

Fig 4.8 Variation of emission intensity with gas velocity for 300 PP and BPP particles
(applied voltage of 7 kV and detected at (x, y) = (0 cm, 0 cm) point)

To compare the detail of the changes of emission intensity, Fig 4.8 presents the variation of emission intensity with the gas velocity with 7 kV applied voltage at the detected point of (x, y) = (0 cm, 0 cm). As can be well known that the emission intensity without particles was gradually decreased with gas velocity. As the presence of PP particles, the emission intensity increased with the increase of gas velocity. Then the emission intensity value reached the highest at the gas velocity around 9.9 m/s, which is the u_{ms} for 300 particles. After reaching the highest value, the emission intensity decreased significantly with gas velocity. All the emission intensity of PP

particles was higher than no particles. However, in the case of BPP particles, the emission intensity even less than that of without particles. The emission intensity with BPP particles kept stable with the increase of gas velocity until 12.4 m/s. After reached the highest value of emission intensity, there was a slight increase with the gas velocity. The highest values of emission intensity for PP and BPP particles were related to the good fluidization behavior at the gas velocity of u_{ms}.

In principle, the concentration of species gives a proportional effect on the emission intensity of discharge gas[12]. Zhang et al.[13] reported that the electron temperature was decreased with the gas velocity. In the literature, two receivable explanations have been given for the reason for gas velocity on the electrical discharge characteristics. Pavon et al.[14] noted that a very high gas velocity resulted in the energetic charge losses and Li et al.[15] explored that heating flowing caused by gas flow also affected on discharge characteristics. If the gas velocity below 100 m/s, it is reasonable to discard the effect of charge losses caused by the high-speed gas flow (Wei et al.[11]). In our case, even the maximum value of gas velocity is also lower than 100 m/s. So, the charge losses during the process can be neglected in this research. In the comparison of high-speed images and the emission intensity data, it is worth to notice that the particle fluidization behavior gave influence on the plasma emission intensity. The variation trend for the emission intensity with gas velocity was consistent with pressure drop, especially for PP particles. The highest value of emission intensity was related to the fluidization behavior. The distance between particles became large with the gas velocity, but too high gas velocity also related to the intense fluidization with significant distance. Based on the high-speed camera images shown in Fig 4.7,

due to the benign collision between electrons and particles, the plasma emission intensity was

enhanced around u_{ms}. In the case of BPP particles, the emission intensity was lower than that

without particles since the absorption by the black surface as we mentioned in 4.3.3. Even though,

the emission intensity also increased for BPP particles with good fluidization behavior.

4.3.5 Effect of particle numbers on the plasma characteristics

(a) 0 particle   (b) 100 PP particles   (c) 300 PP particles   (d) 500 PP particles
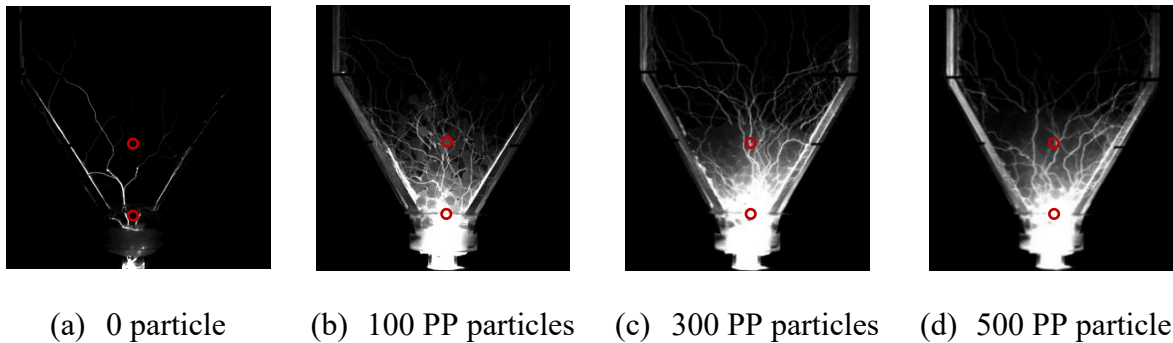
Fig 4.9 High-speed camera imaging of fluidization of different particle numbers

(gas velocity : 9.9 m/s, applied voltage : 7 kV, and frame rate : 750/s)

To future confirm the effect of particles addition on the emission intensity of plasma, different

numbers of the particles were considered with 7 kV applied voltage. Fig 4.9 (a) to (d) reveal the

high-speed camera images for 0, 100, 300, and 500 PP particles with the same gas velocity of

9.9 m/s (u_{ms} for 300 particles). Under the same gas velocity, fluidization behavior varied with

particle numbers. As the gas velocity of 9.9 m/s, 100 PP particles reveal as the intensive

fluidization with a considerable distance between particles. The whole 300 PP particles began to

move with the gas velocity of 16.8 L/min. However, 500 PP particles kept as the fixed bed with

a slight movement for the bottom of the solid bed with this gas velocity. In the case of 200 PP

particles, the fluidization behavior showed the central tendency between 100 and 300 PP

particles. In the case of with 400 particles, only part of particles moved with an area of brightness

shrinker than that of 300 particles. In the comparison of images in Fig 4.9, plasma brightness just showed as several photon lights without particles. However, with the addition of particles, the brightness region enhanced significantly. The region area with significant brightness presented the biggest with 300 PP particles. It is easy to see that the fluidization behavior with different particle numbers effects on the plasma optical characteristics as well.
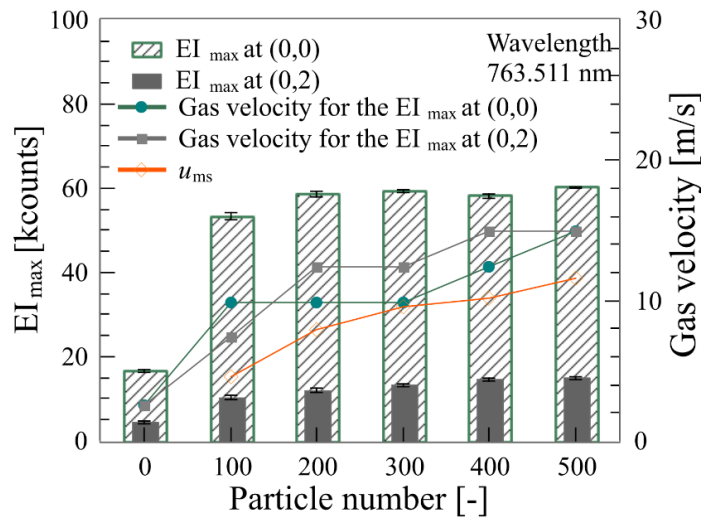

Fig 4.10 Variation of emission intensity with gas velocity for various particle numbers of Ar band (Applied voltage: 7 kV)

$((0, 0)$ relates to $(x, y) = (0$ cm, 0 cm$)$, and $(0, 2)$ relates to $(x, y) = (0$ cm, 2 cm$))$

To compare the difference of emission intensity varies particle numbers, two detected points have been chosen as marked by the red circles in Fig 4.9. The detected point of $(x, y) = (0$ cm, 0 cm$)$ is the point at plasma jet nozzle inlet. Moreover, the point of $(x, y) = (0$ cm, 2 cm$)$ is the same as the initial bed height of 300 particles. Regardless of particle numbers and detected points, the emission intensities changing with gas velocity presented similar trends as shown in Fig 4.8. To future analyze the effect of particle numbers on the emission intensity, Fig 4.10 depicts the changes of the max value of emission intensity (EI_{max}) and the corresponding gas velocity with

various PP particle numbers at the two detected points. EI_{max} is the highest value of plasma emission intensity in the process of increasing gas velocity. When the EI_{max} presented, the gas velocity for EI_{max} with the change of particle numbers also illustrated in Fig 4.10. With the increase of particle numbers, the EI_{max} increased significantly from 0 to 100 PP particles regardless of detected points. At the point of (x, y) = (0 cm, 0 cm), the EI_{max} kept stable from 100 to 500 PP particles. However, the EI_{max} increased with a tiny slope with particle numbers from 100 at the point of (x, y) = (0 cm, 2 cm). The EI_{max} at the point of (x, y) = (0 cm, 0 cm) were almost 6 times than that of (x, y) = (0 cm, 2 cm) regardless of particle numbers. Compared to the gas velocity for the EI_{max}, it is worth noting that an approximately linear relationship between the gas velocities for EI_{max} and particle numbers can be found. The gas velocities for EI_{max} were increased with particle numbers for two detected points. Besides, the gas velocities for EI_{max} were proportional to the value of u_{ms}. The value of EI_{max} presented when the gas velocity passes the u_{ms}.
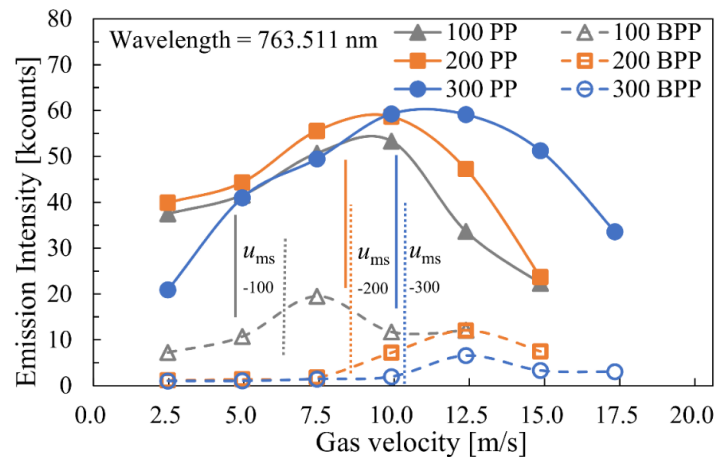

Fig 4.11 Variation of emission intensity with gas velocity for various types of particles

(u_{ms} lines: solid lines for PP particles, and dotted lines for BPP particles)

(applied voltage of 7 kV and detected at (x, y) = (0 cm, 0 cm) point)

As we know, the particle numbers increased lead to enhance the initial pressure drop of solid bed, which means the drag force was much high with adding more particles. The fluidization behavior is different under the same gas velocity. It should be mentioned that the plasma emission intensity also related to the particle fluidization behavior. When the gas velocity higher than u_{ms}, there was a period for particles fluidizing so well. The high value of emission intensity can be obtained with the good fluidization behavior of particles, regardless of particle numbers and detected points. Proper fluidization provided a suitable distance between particles and led to the good movement for particles, which enhanced the collisions between plasma and particles.
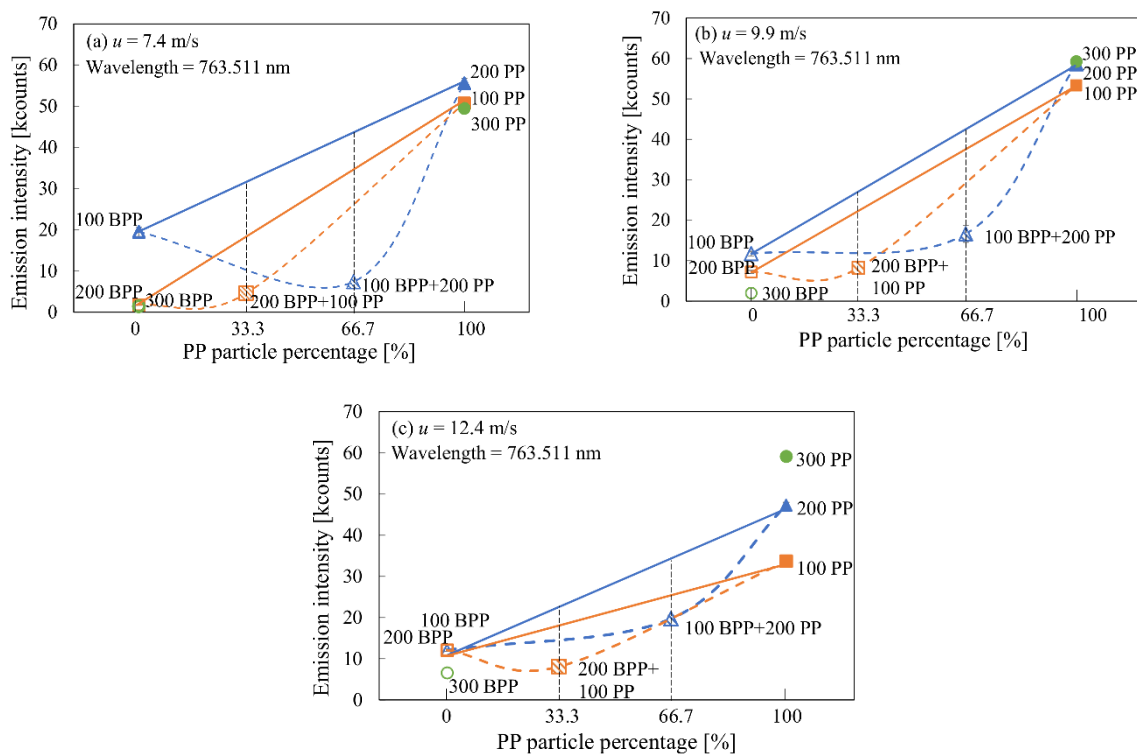

Fig 4.12 Variation of emission intensity with mixture particles of PP and BPP

(applied voltage of 7 kV and detected at (x, y) = (0 cm, 0 cm) point)

Based on the above data, the emission intensity with BPP and PP particles were different. The diameter and density of PP and BPP particles were similar, that result in less influence on the

difference of fluidization behavior. To achieve a better understanding of the relationship between emission intensity and particle types, Fig 4.11 presents the emission intensity changed with PP (solid markers) and BPP (hollow markers) particles with three particle numbers. In the case of mixing the PP and BPP particles, the voltage was applied after the proper mixing by gas. The whole trends for two kinds of particles were similar that the gas velocities for EI_{max} corresponded well with u_{ms}. The solid lines refer to the u_{ms} for the PP particles, and dotted lines refer to the BPP particles. However, with the 100 BPP particles, the full values of emission intensity were higher than other numbers of BPP particles.

To compare the difference of emission intensity for particle type, we compared the mixture particles of PP and BPP particles with different gas velocities, some of the data showed in Fig 4.12. The hollow markers refer to the data with BPP particles and solid markers refer to the data with PP particles. The data for the mixture of PP and BPP particles showed as the pattern markers. The emission intensities with more BPP particles were less than that with a small amount. With the increase of gas velocity, the gap between various particle number decreased. For PP particles, there were no apparent changes between the three numbers. However, the difference in emission intensity with particles increased so much as the gas velocity to 12.4 m/s. The emission intensity data for mixture particles were not as a simple calculation result regardless of the gas velocity. With the addition of BPP particles, the emission intensity of plasma declined significantly regardless of the gas flow rate. More percentage of PP particles added in the mixture particles presented the relatively high emission intensities. The emission intensity of plasma with mixture particles increased slightly by the gas velocity. In the mixture of PP and BPP particles, due to the

addition of BPP, the emission intensity not increased as a line relationship with the standard calculation. As we mentioned before, due to the difference in the material and electrical conductivity of BPP and PP particles, the plasma characteristics were different. However, in the mixture of particles, the emission intensity declined significantly. It can be assumed that the effect of absorption of BPP particles on the detected emission intensity is significant.

4.4 Summary

A combination of DBD plasma jet with a two-dimensional spouted bed process has been established in this chapter. The optical emission spectral characteristics of Ar plasma and the effect of fluidization behavior on the optical emission spectral characteristics were investigated by changing the parameters of particle types, applied voltages, gas velocities, and particle numbers. This chapter extends the theoretical framework of our previous research that analyzed the effect of plasma irradiation on the particle's fluidization behavior. The main conclusions are as followed.

1) The plasma irradiation had changed the fluidization behavior of particles. With the presence of Ar plasma irradiation, the pressure drops for PP particles were decreased but not for BPP particles.

2) The emission spectra of Ar plasma had been changed significantly with the addition of particles. The atomic spectrum of Ar I and II transition lines for Ar plasma was detected without particles. However, the transitions of Ar II lines were decreased by the addition of particles. The emission spectrum of Ar I was enhanced with PP particles and declined with BPP particles. A

high concentration of excited and ionized (active) plasma species was produced due to the presence of particles for enhancing collisions with each other.

3)   The emission intensity of Ar I lines was enhanced with the voltage applied regardless of the addition of particles. There was a linear relationship between the applied voltage to the emission intensity for most of the wavelengths of Ar I lines from 4 kV to 7 kV. The enhancement of emission intensity with PP particles was more than 5 times than that of no particles.

4)   The changes of emission intensity with gas velocity were different between with and without particles. The emission intensity was decreased slightly with the gas velocity when no particle was added. However, as the presence of particles, the emission intensity with gas velocity changed in accord with the fluidization behavior of particles.

5)   The emission intensity of plasma versus particle numbers was identified with fluidization behavior. The high value of emission intensity can be obtained with the good fluidization behavior of particles regardless of particle numbers and detected points. The emission intensity of mixture PP and BPP particles was not the calculated data by the pure particles. The difference between color and electrical conductivity between BPP and PP particles may be resulting in the distinction on detected emission spectral data and pressure drop.

In summary, two kinds of parameters can be affecting the high emission intensity of plasma state: enough supplied energy by a high applied voltage, the suitable distance between particles by a good fluidization behavior which related to the gas flow rate and the number of added particles. Notably, the fluidization behavior of particles had an essential role in the changes in emission intensity. The difference in the color of particles regarding the absorption and reflection

rate of lights gave influence on the detected emission spectral data. Moreover, the changes in pressure drop with high applied voltage may be affected by the distinction of particle electrical conductivity. Our findings suggest that a promotion of plasma emission intensity by particles fluidization that might provide a viable source for the process, such as the process of plasmatic pollutant disposal with the catalysts. However, further studies are needed to determine the detail for the effect of particles electrical conductivity on the fluidization and plasma optical emission spectral characteristics.

4.5 References

[1].Gao et al., "Optical emission spectroscopy diagnosis of energetic Ar ions in synthesis of SiC polytypes by DC arc discharge plasma," Nano Res., vol. 11, no. 3, pp. 1470–1481, 2018.

[2].M. V. Malyshev and V. M. Donnelly, "Determination of electron temperatures in plasmas by multiple rare gas optical emission, and implications for advanced actinometry," J. Vac. Sci. Technol. A Vacuum, Surfaces, Film., vol. 15, no. 3, pp. 550–558, 1997.

[3].B. Zhang, N. Kobayashi, and Y. Itaya, "Effect of plasma irradiation on the fine particle behavior in a spouted bed," Powder Technol., vol. 343, pp. 309–316, 2019.

[4].R. Pissinati and W. P. Oliveira, "Enteric coating of soft gelatin capsules by spouted bed: effect of operating conditions on coating efficiency and on product quality," Eur. J. Pharm. Biopharm., vol. 55, no. 3, pp. 313–321, May 2003.

[5].B. Krause and P. Pötschke, "Electrical and thermal conductivity of polypropylene filled with combinations of carbon fillers," AIP Conf. Proc., vol. 1779, no. October 2016, pp. 1–6, 2016.

[6].S. Morooka, K. Kusakabe, A. Kobata, and Y. Kato, "Fluidization state of ultrafine powders," J. Chem. Eng. Japan, vol. 21, no. 1, pp. 41–46, 1988.

[7]."NIST Atomic Spectra Database Lines Form," 2018. [Online]. Available: https://www.nist.gov/pml/atomic-spectra-database.

[8].S. K. Lam et al, "Kinetics of Ar * 2 in high-pressure pure argon," J. Phys. D. Appl. Phys., vol. 33, no. 3, p. 242-, 2000.

[9].ZHANG, X. BIAN, Q. CHEN, F. LIU, Z. LIU, "Diagnosis of Methane Plasma Generated in an Atmospheric Pressure DBD Micro-Jet by Optical Emission Spectroscopy," CHIN. PHYS. LETT., vol. 35203, 2009.

[10].R. Zaplotnik et al., "Multiple vs. Single harmonics AC-driven atmospheric plasma jet," Epl, vol. 106, no. 2, 2014.

[11].G. D. Wei, C. S. Ren, M. Y. Qian, and Q. Y. Nie, "Optical and electrical diagnostics of cold Ar atmospheric pressure plasma jet generated with a simple DBD configuration," IEEE Trans. Plasma Sci., vol. 39, no. 9, pp. 1842–1848, 2011.

[12].N. U. Rehman, F. U. Khan, N. A. D. Khattak, and M. Zakaullah, "Effect of neon mixing on vibrational temperature of molecular nitrogen plasma generated at 13.56 MHz," Phys. Lett. Sect. A Gen. At. Solid State Phys., vol. 372, no. 9, pp. 1462–1468, 2008.

[13].Z. Jun-Feng, B. Xin-Chao, C. Qiang, L. Fu-Ping, and L. Zhong-Wei, "Diagnosis of Methane Plasma Generated in an Atmospheric Pressure DBD Micro-Jet by Optical Emission Spectroscopy," Chinese Phys. Lett., vol. 26, no. 3, p. 35203, Mar. 2009.

[14].S. Pavon, J. L. Dorier, C. Hollenstein, P. Ott, and P. Leyland, "Effects of high-speed airflows

on a surface dielectric barrier discharge," J. Phys. D. Appl. Phys., vol. 40, no. 6, pp. 1733–1741, 2007.

[15].S. Z. Li, W. T. Huang, and D. Wang, "The effect of gas flow on argon plasma discharge generated with a single-electrode configuration at atmospheric pressure," Phys. Plasmas, vol. 16, no. 9, 2009.

5. Fluid Dynamics of Particles in an AC DBD plasma-enhanced Spouted Bed

5.1 Background

In the previous chapters, it is well accepted that the good fluidization behavior effected on the plasma irradiation. At the same time, the emission intensity of plasma was also altered with the fluidization behavior. However, the fundamental understanding of the fluid dynamics for solid particles in the plasma-enhanced system is still incomplete. While in the practical application, such as the catalytic pollutant removal system, it is essential to control the reaction efficiency by mastering the fluid dynamics of particles, especially with the plasma irradiation.

The particles fluid dynamics was performed by the acting forces between particles and plasma gas. The gas discharge generated the electron-ion pairs through the electron impact from the ionization of the gas in the plasma system[1]. The ions and electrons can charge the solid particles from the air due to the plasma irradiation[2]. Plasma acted on the charged particles with the electrohydrodynamic (EHD) force in a gas-solid system. While a strong external electric field existed, a body force "pushed" [3][3] on the external gas[4][5], which also leads to the thrust force for charged particles. The electrohydrodynamic (EHD) [2] by the plasma irradiation was mainly showed as the electric field force for the charged particles. Here, the electric field force (F_E) and body force with a consistent expression that is given below:

$$F_E = \rho_c E \qquad \text{Eq. (5-1)}$$

Where ρ_c represents the charge density of particles and E represents the electric field.

The force caused by the ion drift with the along or counter to the free-stream flow direction was confirmed through the smoke visualization by particle image velocimetry (PIV) method in Sung's research[6] for a wall-surface AC-DBD plasma actuator. Results revealed that the wake of flow after the cylinder became narrowing at the high discharge voltages, and the suction effect was presented close to the electrodes when the flow configuration was stagnated.
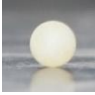
This chapter extends the theoretical framework and focuses on the particle dynamics by particle image velocimetry (PIV) and particle tracking velocimetry (PTV) methods in an AC-DBD plasma-enhanced spouted bed system. PIV method, as the non-invasive technique, was applied to study the particle behavior[7][8] in a fluidized bed and plasma behavior in the actuator[9][10]. PTV method was used to identify the individual particles in images[11]. It is feasible to investigate the relationship between the plasma parameters and the flow structures formed in the system by these techniques without disturbing the flow field. Herein, to examine the particle dynamics in a DBD-enhanced spouted bed system, several parameters were changed, including fluidization parameters (gas velocity, particle numbers, and particle type), and plasma parameter (applied voltages). The effect of plasma irradiation on the fluid dynamics was obtained from the analysis by Flow Expert 2D2C software through the images taken by a high-speed camera.

5.2 Experiments and conditions

Fig 2.2 presents the details of the plasma jet nozzle and the location of detection machines. In this chapter, Polypropylene (PP) particles were the primary fluidized agent with a diameter of 3

mm and a density of 897 kg/m^3 to obtain the velocity profile of particles in the plasma-enhanced

spouted bed.   Polyamide (PA) particles with the same diameter and 1140 kg/m^3 in density were

adopted to figure out the mechanism of particles dynamics in this system. The dielectric constant,

a quantity measuring the ability to store electrical energy in the electric field, is different for PP

and PA particles (1.5 for PP, and 2.5 for PA). Several parameters (as shown in Table 5.1), which

gave an influence on the emission intensity of plasma significantly in previous paper, such as the

number of particles (difference on initial pressure drop, from 1 to 500), and the Ar gas velocity

(u, from 7.4 to 14.9 m/s) were changed to indicate the particle dynamics at various fluidization

behavior with the effect of applied voltage (U, 0 and 7 kV) in this system.

Table 5.1 Research process conditions

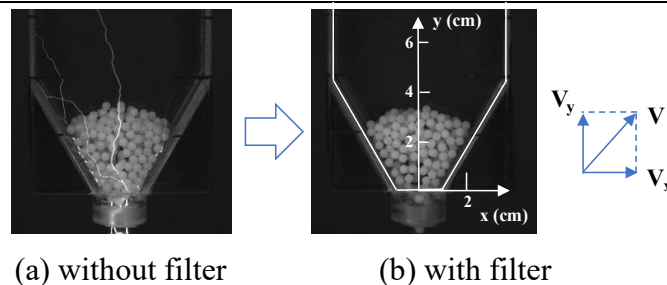| Category	Symbol	Unit	Variables	
Particle type	–	–	PP particles	PA particles
Particle number	–	–	0 – 500	
Applied voltage	U	kV	0 – 7	
Flow rate	u	m/s	7.4 - 14.9	

(a) without filter   (b) with filter

Fig 5.1 The characteristics of particle flow pattern in a spouted bed.

(a)Without filter settled and (b) with filter settled

(gas velocity:9.9 m/s and the number of particles: 300 PP).

The motion of particles in the plasma-enhanced spouted bed showed in Fig 5.1(a), which was taken by a high-speed camera (FASTCAM MiniAX100, Photron). The imaging system was controlled through the software of FASTCAM Viewer 3 (Photron). Significant plasma filament lights can be found clearly in the picture. To observe the movement in the full view, we settled two webs of led photo lights (L18582-1, LPL) in front of the spouted bed. Due to the presence of plasma light affect the accuracy when analyzing the motion by PIV and PTV methods through the analysis in the software of Flow Expert 2D2C software (Kato Koken), a UV-IR-CUT filter (slim, 72 mm, Haida) was used before the camera lens to remove the influence of plasma light on the images. Fig 5.1 (b) shows the image with the filter installed on the camera. Due to the particle velocity changed drastically by the collision with other particles and spouted wall, the frame rate of camera determined by the displacement of a particle in two sequential images which should be less than the particle radius[12]. All the images were operated with a frame rate of 10000 fps and a resolution of 768×528 pixels. The interval time is 1 ms, and the interval grid is 2 × 2 mm. Then analyzing the photos, the coordinate direction of the spouted bed has been analyzed as Fig 5.1 (b) presented. x is the transverse coordinate centered about the jet, and y is the distance from the jet inlet. The average particle velocity profile data was calculated by analyzing 1000 images with a duration time of 1 s in the experiment.

The plasma feature evaluated as the optical emission spectroscopy (OES), by a spectrometer (FLAME-S, Ocean Optics) and an optical fiber (P600-1-SR, Ocean Optics) with a wavelength of 200 to 886 nm and an integration time of 1 s. The probe settled in front of the spouted inlet

with 3 cm and noted as (x, y) = (0 cm, 0 cm). The point of (x, y) = (0 cm, 0 cm) is the original

point for the spouted bed, which was just above the plasma jet nozzle.

5.3 Results and discussion

5.3.1 Fluidization behavior
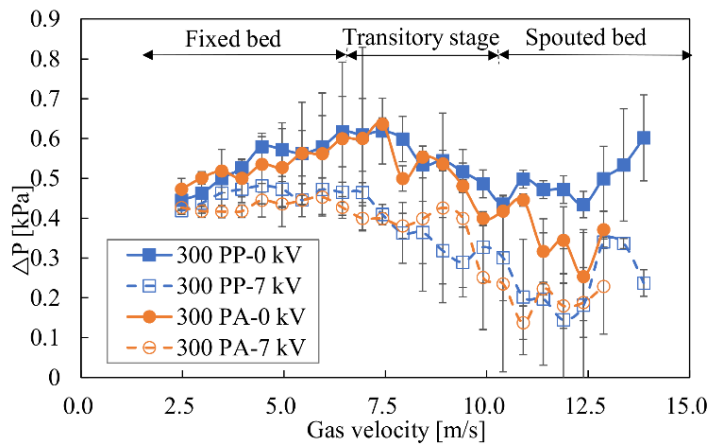
Atem	u_{ms}* [m/s]
PP particles - 0 kV	9.9
PP particles - 7 kV	9.5
PA particles - 0 kV	10.4
PA particles - 7 kV	10.1

*: u_{ms} in this paper.

Fig 5.2 Variation of pressure drop with Ar gas velocity for 0 kV and 7 kV applied voltage.
(Solid line refers to the case of without plasma irradiation, and the dotted line refers to the
case with 7kV applied voltage.)

It is essential to obtain the fluidization behavior of particles by analyzing the pressure drop

(ΔP) of the solid particle changing with the gas velocity firstly. Fig 5.2 illustrates the typical

trends of pressure drop for 300 particles with an increase of Ar gas velocity. The trends for

pressure drop are similar for PP and PA particles, which increased in the initial stage with the

gas velocity that the solid particles maintained as the fixed bed. With the increase of gas velocity,

the bottom part of particles started to move slightly, leading to the decline on the ΔP which

regarded as the transitory stage. When the gas velocity increased around minimum spouted

velocity (u_{ms}), particles started to be spouted among the whole solid bed. As the gas velocity just exceeded the u_{ms}, the particles circulated smoothly in the spouted bed. The particles moved with an absolute amplitude as the gas velocity increased further. Due to the density of PA particles were higher than PP particles, the u_{ms} for PA is large. As the dotted lines showed, with the 7kV applied voltage, the pressure drop of particles was declined both for PP and PA particles. However, even the pressure drop was declined drastically with 7kV applied voltage; the u_{ms} decreases slightly as illustrated in the table. The u_{ms} for 300 PP particles was 9.9 m/s without plasma irradiation. However, with the 7 kV applied voltage, the u_{ms} decreased to 9.5 m/s.

5.3.2 Particle velocity profiles for PP particles

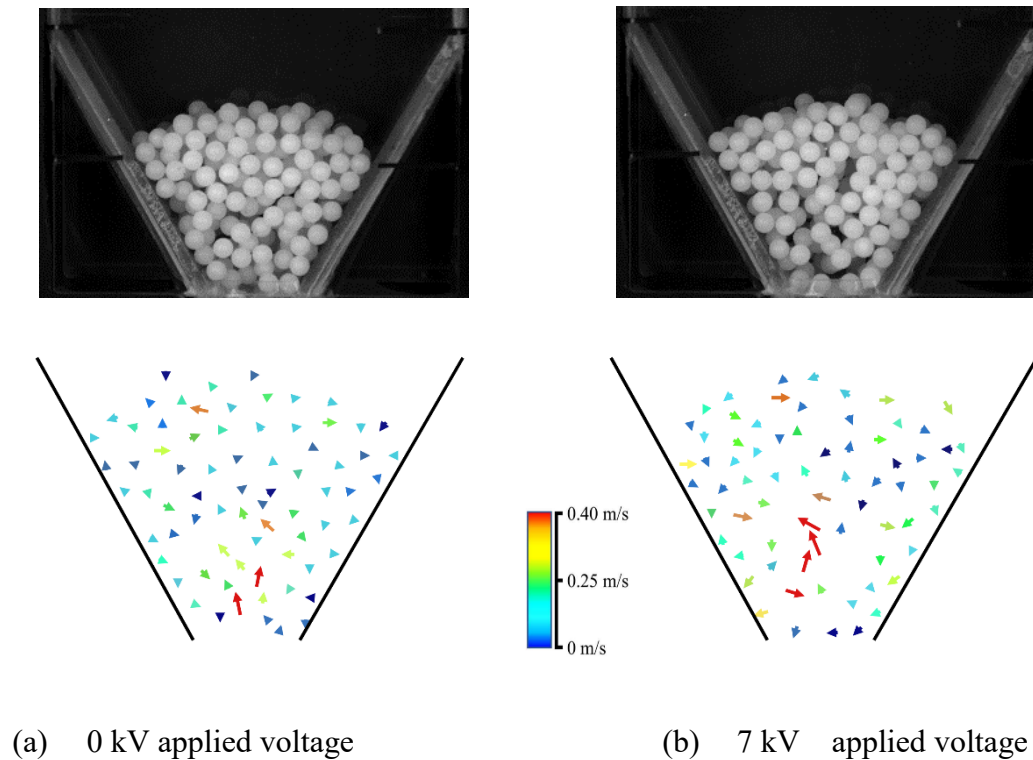(a)   0 kV applied voltage   (b)   7 kV   applied voltage

Fig 5.3 Time-averaged particle velocity fields

(gas velocity: 12.4 m/s, number of particles: 300 PP).

To get a complete view of particle movement, we showed the maps of velocity vectors in Fig 5.3 and Fig 5.4. Fig 5.3 (a) - (b) reveal the examples of the particle tracks with the time-averaged PTV method in a case of 300 PP particles with a gas velocity of 12.4 m/s which just over u_{ms}. The arrows represent the velocity direction of particles. The color of arrows showed the velocity magnitude. There was a fountain-shaped distribution for the particle velocity vectors around the spouted bed inlet angle. The space between particles was larger with 7 kV applied voltage than without plasma irradiation, which means the bed expanded slightly with the plasma irradiation. Even though here we just presented a couple of pictures, we can also mentioned that more arrows with high velocities (red color) can be found in the case with 7 kV applied voltage. The highest velocities, with a magnitude of ten times than other parts, appeared in the upper part of the fountain, not at the inlet part.
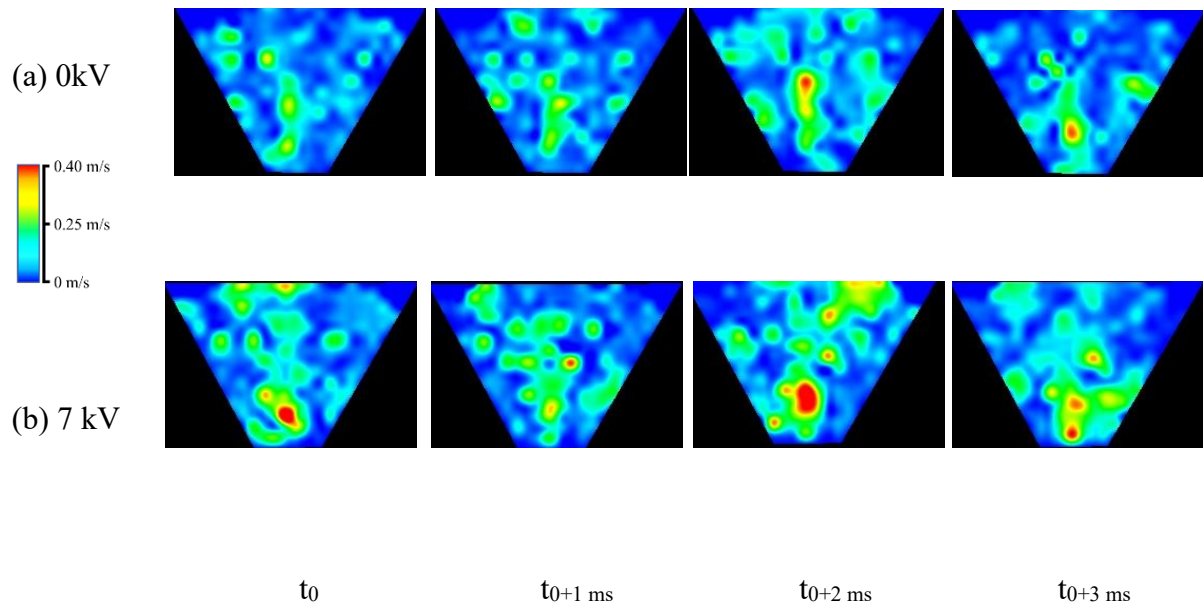

Fig 5.4 Instantaneous distribution of the particle velocity (a) with 0 kV applied voltage and (b)with 7 kV applied voltage (gas velocity: 12.4 m/s, number of particles: 300 PP).

To get further insight of particle velocity field, we adopted the PIV method to compare the velocity vectors with 300 PP particles. The velocity vector profiles without applied voltage (Fig 5.4 (a)) and with 7 kV applied voltage (Fig 5.4 (b)) showed a similar trend. The same pattern can be found as PTV data (as shown in Fig 5.3) that irrespective of the voltage applied, the particles in the spouted bed moved with high speed above the inlet part of the plasma jet nozzle. The particles with the high velocity presented along the central line regardless of plasma irradiation. When the 7 kV voltage applied (the figures in the second line), the large area of particle velocity with more than 0.25 m/s (the area with red and green color) were presented.
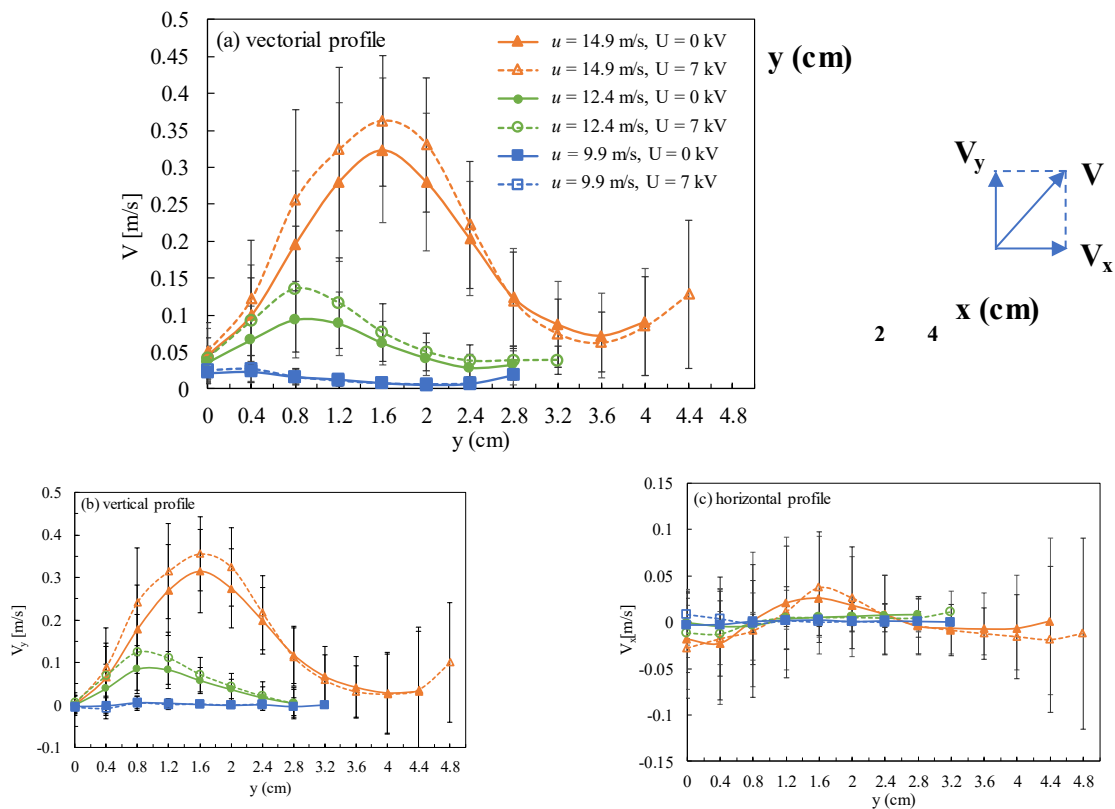

Fig 5.5 Experimental profiles of particle velocity in the spouted bed along spout axis versus several gas velocities (a) vectorial profile, (b) vertical profile, and (c) horizontal profile (number of particles: 300 PP, x at 0 cm).

To confirm the changes of particle velocity profile with the addition of plasma irradiation in detail, we compared the particle velocity profile with and without applied voltage in various conditions of gas velocity based on the PIV analysis. Fig 5.5 (a) - (c) show the quantitative comparison of the profile of particle velocity at vectorial (V), vertical (V_y), and horizontal (V_x) direction along the spout centerline (x equal to 0 cm). y represents the longitudinal distance from the inlet of spouted bed. Three superficial gas velocities (u) were changed from 9.9 m/s (u_{ms} for 300 PP particles) to 14.9 m/s (fluidized without intensive movement). The same initial static height of 300 PP particles was fixed as the constant of 2.0 cm.

The axial development of the velocity profile at the vectorial direction showed in Fig 5.5 (a). The whole trends for particle velocity with the increase of y were similar. As would be expected, the vectorial particle velocity increased with the y distance; then the highest velocity appeared with a peak at the upper part of the solid bed. In the top part of the solid bed, the particle moved with a low velocity. All the value of particle velocity for V and V_y are the positive value that means the particles moved along the upward direction at the centerline. The maximum value of vectorial velocity (V_{max}) and vertical velocity ($V_{y\text{-}max}$) also increased with superficial gas velocity noticeably. Take a full view of the velocity profile, and the Vy-max presented in the central of the solid spouted bed that in the tunnel part of the fountain. As can be seen in Fig 5.5 (c), the Vx changed with a little value at the y distance even though with high superficial gas velocity. Some negative value of V_x (Fig 5.5 (c)) with the big error bar can be found which due to the random move direction of particles.

As would be expected, the particle velocity among gas-phase centerline increased first and then decayed with axial distance. It could be expected that centerline velocity was increased as momentum, which was transferred from the jet gas to the particles via drag[13]. It seems that the particles accelerated slowly at the inlet, and then moved quickly in the upper part of the fountain, due to the cross-sectional area of the annulus changed small[14] upon the inlet. However, the velocity of particles decelerated gradually at the top of the fountain. The value of V and Vy preented a high peak and a sizeable high-velocity region at the central part of the fountain. In Liu's research[14], a long flat peak of the velocity profile of the highest value with initial high bed height was obtained in a 2D spouted bed. He pointed out that a flat peak of velocity profile was shortened with decreasing the initial bed height in a spouted bed reactor. However, in our case, the initial bed height is not high enough to present a flat peak.

Compared to the case with the 7 kV applied voltage as the dotted line showed in the figures, there was a noticeable improvement for the V and V_y with plasma irradiation. It means that the increase of particle velocity in the y-direction mainly caused the enhancement of the velocity profile. The enhancement of particle velocity is different with the gas velocity that enhancement of particle vectorial velocity changed from 45% (12.4 m/s of gas velocity) to 12% (14.9 m/s of gas velocity). It should be noted that at 14.9 m/s of gas velocity, the $V_{x\text{-}max}$ moved to the upper part of solid bed than the case without applied voltage. The detailed reason for the plasma irradiation resulting in the enhancement of velocity, especially in the vertical direction will be discussed later.
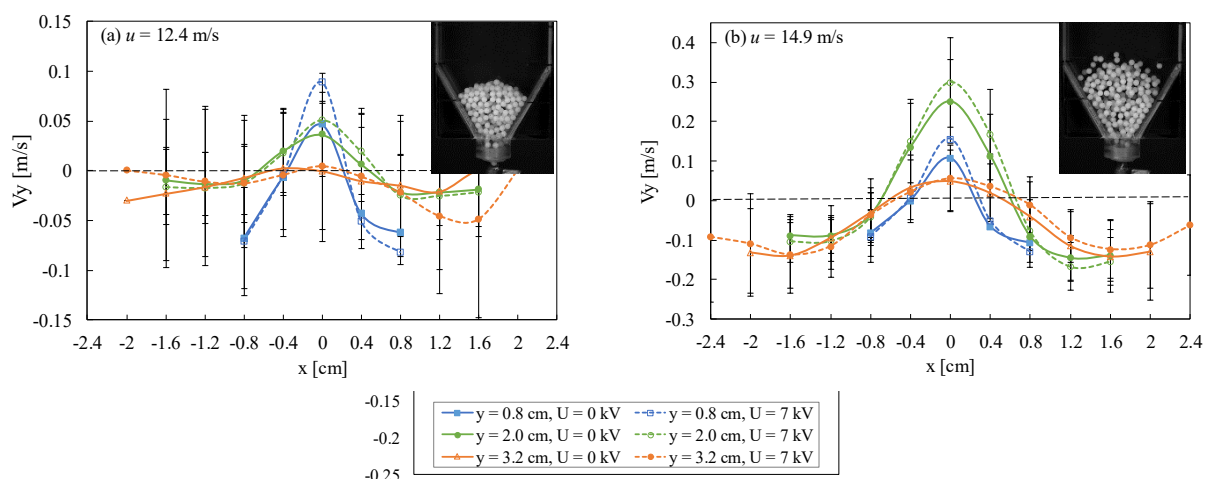
Fig 5.6 Profile of vertical particle velocity at lateral direction in the spout at various bed levels and superficial gas velocity (a) gas velocity of 12.4 m/s and (b) gas velocity of 14.9 m/s (number of particles: 300 PP).

Further, due to the upward movement of particles at the spout centerline in spouted bed, V_y was adapted to show the changes in the lateral direction. Fig 5.6 (a) - (b) illustrate the V_y at the lateral direction (x-direction) in the spouted bed with two superficial gas velocities at various height locations. The V_y decreased from its maximum at the central region to the conical bed wall irrespective of the locations on the y-axis. As the low superficial gas velocity (12.4 m/s), it is noted that Vy-max of particles decreased with the increase of vertical level (y). However, as the superficial gas velocity with a high value (14.9 m/s), the V_{y-max} value appeared in the middle part of the fountain, which agreed with the data in Fig 5.5. When plasma irradiation added, almost of V_y absolute values were enhanced, especially at the low position of solid bed (blue lines and green lines). The effect of gas velocity on the particle velocity profile was significant. The enhancement of V_y with plasma irradiation showed as 91% while y equal to 0.8 cm, and 40% at y equal to 2.0 cm with the gas velocity of 12.4 m/s. However, the enhancement of V_y decreased to 45% and 19% at the same position with the gas velocity of 14.9 m/s. The difference in the

distribution was related to the fluidization behavior, which can be found from the images in each

condition. More space can be found among particles with high gas velocity.

5.3.3 Effect of particle type and particle number

As mentioned above, the whole distribution of velocity was enhanced with 300 PP particles

addition as 7 kV voltage applied, especially with high superficial gas velocity. Another agent of

PA particle was adopted here to compare the difference for particle type. A similar trend (as

shown in Fig 5.5 and Fig 5.6) of velocity distribution with the same particle number for PA

particles, with the same diameter but different density to PP particles, was obtained. However,

there was a difference in the particle velocity profile for PA particles that the whole velocities

were much lower than that of PP particles at the same gas velocity due to the high particle density.
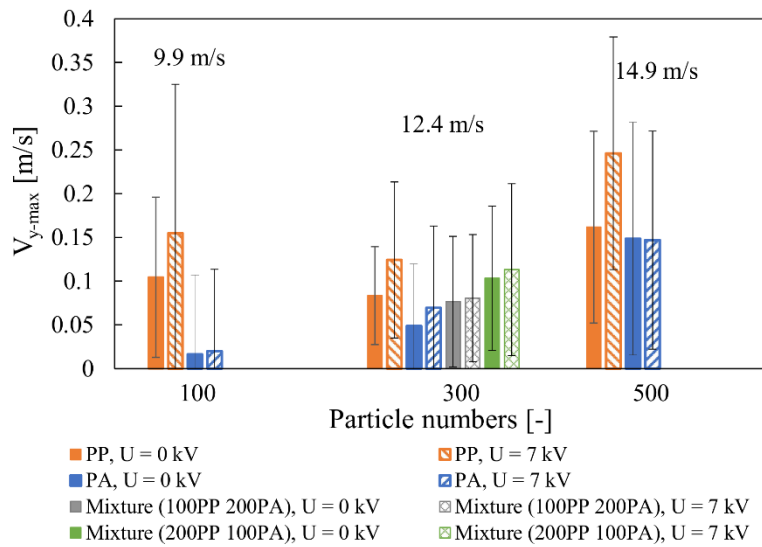

Fig 5.7 Relationship of $V_{y\text{-}max}$ and particle number various particle types

To gain more insight into the velocity distribution of particles, particle number for two kinds

of fluidized particles were changed in this section. Fig 5.7 illustrates the effect of particle

numbers on the maximum value of vertical velocity ($V_{y\text{-}max}$) in the velocity profile for pure

particles and well-mixed particles of PP and PA particles. In our previous study, we found that the highest emission intensity had been changed with the particle numbers and the gas velocities. The highest values of emission intensity presented just above the gas velocity of u_{ms}. To achieve the relatively consistent of fluidization behavior and the plasma irradiation, we adopted the gas velocities (above u_{ms} for each condition, which corresponding displayed in Fig 5.7) responding to a good fluidization behavior and the highest values of emission intensity. The values of $V_{y\text{-max}}$ for PA particles were increased with particle numbers obviously, but not for PP particles. The $V_{y\text{-max}}$ was improved with the 7 kV applied voltage in most cases for PP and PA particles. Notably, the enhancement of $V_{y\text{-max}}$ for PP particles with 7 kV applied voltage was almost stable around 50% which was much higher than that of PA particles. The most significant improvement of $V_{y\text{-max}}$ by the plasma irradiation for PA particles was 43% with 300 particle number. Especially in the case of 500 PA particle, the data for the $V_{y\text{-max}}$ almost the same with 0 kV and 7 kV. The location of $V_{y\text{-max}}$ presented to a higher location with 7 kV applied voltage in the case of 100 PP, 100 PA, and 500 PP. In other cases, the location of $V_{y\text{-max}}$ almost no change, which not consistent with the images illustrated in Fig 5.3 and Fig 5.4. Besides, the variation of the $V_{y\text{-max}}$ with a mixture of PP and PA particles, with a total number of 300, also be demonstrated in Fig 5.7. $V_{y\text{-max}}$ was increased with the PP particle percentage in the mixture of particles. However, based on the average data of mixture particles, the location of particles showed with the $V_{y\text{-max}}$ was almost same with plasma irradiation, not as the pure PP particles. The reason for the location for the highest particle velocity without changes in some cases, maybe due to the grid of 2×2 sm with the average calculation.

5.3.4 Discussion on the changes in particle dynamics

As the presence of plasma, a sizeable high-velocity region of particles can be observed with high gas velocity. The main changes of particles dynamics in a DBD plasma-enhanced spouted bed may be depended on the thermal effect and the force for particles due to the plasma irradiation.

1)   Thermal effect

For the gas phase, Li et al.[15] explored that heating flowing caused by gas flow also affected on discharge characteristics. However, the gas temperature increased slightly here within 20°C measured by an infrared camera (FLIR T440, CHINO) owing to the excited state from the plasma activation. It means that the effect of the temperature on the particle velocity was small. The gas-phase was insufficient for the changes of particles dynamics due to the slight change of density and the viscosity for gas in the ionization process. It corresponds well with the data showed in Fig 5.5 that if the gas density increased, the peak of particle velocity would be presented on the high y position.

Fig 5.8 reveals the variation tendency of the electron temperature (Te) versus the particle type with the same particle number of 300 particles. The electron temperature of Ar plasma was much higher than the conditions with particles. The electron temperature went down due to the electrons undergo inelastic collisions with high intensity and loosed kinetic energy with the addition of particles. It was also corresponded well with the emission intensity of Ar plasma in chapter 4, that the emission intensity enhanced with the presence of particles.   More collision of the electron resulted in the transition process with the release of the photon (emission intensity

was enhanced). However, the trend of electron temperature was not similar to the $V_{y\text{-max}}$, which due to the detected location of electron temperature was at the inlet point not same as the location of $V_{y\text{-max}}$ of particles.
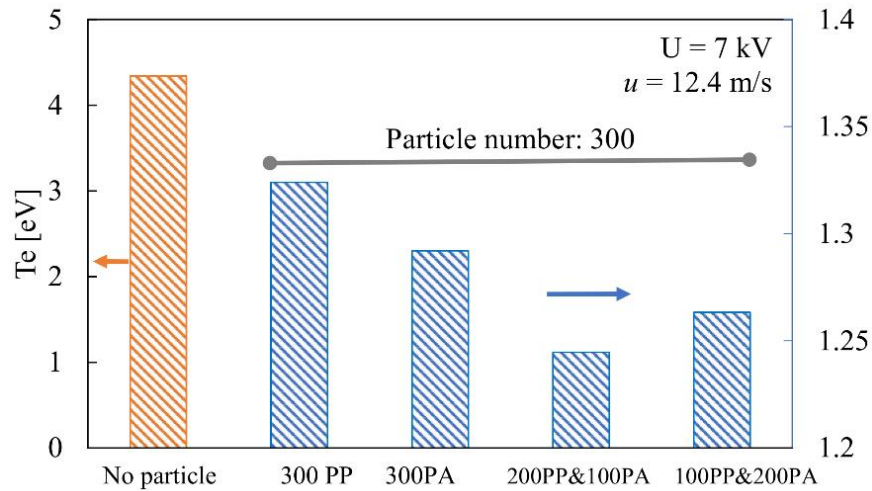

Fig 5.8 Plot of electron temperature versus the particle type at the gas velocity of 12.4 m/s. (Analyzed by Boltzmann's plot of the Ar line spectrum for 357.215, 379.94, 706.7 and 800.616 nm for 300 particles.)

2) Force analysis

On the other hand, the charged particles can be "pushed" by the electrons and ions within the strong electric field. For the solid phase, if each particle is considered as an individual object, the movement of particles can be described by the Newtonian equation. The pressure gradient and temperature kept stable in the system, so the pressure gradient and thermophoresis are neglected. Besides, the magnetic force was neglected in the most analysis with the plasma irradiation; it was not considered. Therefore, the Newtonian equation mainly included the effect of gravity force, contact force and drag force and electric force. The governing equations for the solid phase in the plasma-enhanced system are shown as follows,

$$m_p \frac{d\vec{v_p}}{dt} = m_p g + F_d + F_c + F_E \qquad \text{Eq. (5-2)}$$

In the left side, where m_p represents the mass of a particle, $\vec{v_p}$ represents the particle velocity.

In the right side, where $m_p g$ represents the particle gravity, F_d represents the drag force, F_c represents the contact force, and F_E represents the electric field force.

Since the particle diameter is over 10 μm[16] and with a rough surface, gravity should be considered. Opposed and proportional to particle velocity caused the drag force (F_d), which cannot be neglected in all conditions. The normal and tangential contact force (F_c) contributed to the particle rotation in the fluidization process. These first three terms on the right side of Eq. (5-2) also existed in the fluidization process without plasma irradiation. We herein focused on the effect of electric field force (F_E) on the fluid dynamics changes, which presented in Eq. (5-1).While the fluidized particle also can be charged in the collisional and frictional[17] processes without plasma irradiation. However, to discuss the changes of fluid dynamics by the plasma irradiation, the collisional and frictional charge have not considered here.

In this AC-DBD actuator, the continuous excitation voltage by AC with 20 kHz in this research contributed to the directional movement of ions and short discharge duration (several tens nanoseconds). Also, the charge density as a function of the electric field with a variation of duration. It further affects the electrical energy deposited in the energetic electrons [18]. In the DBD plasma process, the particles were charged dominated with the attachment of electrons and ions from the gas. For the reason of higher mobility of electrons than of ions[19], the particles presented the predominantly negatively charged.
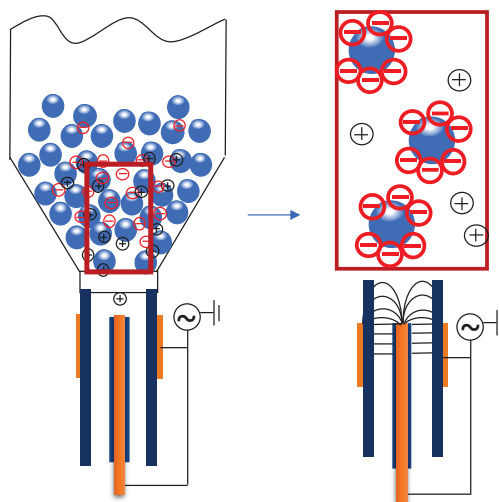
Fig 5.9 Charging mechanism on the particle in the system

The mechanism of the fluid dynamics in the plasma-enhanced spouted bed is assumed and revealed in Fig 5.9. In the enlarged figure, two main electric fields were illustrated. The charged particles were subjected not only in the external electric field but also in the field of accumulation of ion charges on their surface[20][21]. The direction of the electric field was multifarious because of the AC applied. Near the electrode's area, high electric field strength can be found. The axial direction of the plasma jet caused to the discharge configuration in the electrical field, which is parallel to the gas flow direction. So a linear-field plasma jet has been built up, which was confirmed in Wei's paper[22]. The solid bed was expanded with plasma irradiation due to the repulsive force between particles enhanced by the ion accumulation on the surface. The ion drifts led to a net force along the streamwise direction of gas, which further improved the velocity of particle fluidized in the spouted bed. To confirm the existence of the ion charge on the surface by the external electric field, one single PP and PA particle were adopted in a quartz tube replaced the spouted bed (1 m in length and 4.15 mm for inner diameter) with a gas flow rate of 2.2 to 2.6 m/s. Result show with a low gas velocity, the particle maintained stable; however, when the

voltage applied, the particle was pushed up regardless of PP and PA particle. With the increase of applied voltage, the stopped height of the particle was enhanced. The particle and the quartz tube have been charged around 2 kV which was detected by a digital static meter (KSD-1000) with 1 mm distance between the static meter and particle.

With the increase of gas velocity, the mechanism model in the system has been changed with the fluidization of particles. As the gas velocity lower than u_{ms}, particles maintained as the fixed bed contacting with each other. Due to the polarization of the particles[21], the enhancement of electric field strength was much high at the contact points (or the position of the smallest void channel), which regarded as "contact point model[23] ". With the increase of gas velocity ($u>u_{ms}$), the gap size between particles has been enhanced. The electric field transmitted from the "contact point model" to the mix of the "channel of void model[23] " and the "contact point model. " Even though the electric field near the contact point of particles was decreased at the gas velocity of u_{ms}, the electric field was easy to cover the whole gas gap. The electric field was deceased with the increase of particle gap, in combination with our results in previous, too much gap size was also not benefited to the emission intensity of plasma. Thus, it is essential to obtain a suitable balance point for the utilization of plasma source, that the gas velocity is around u_{ms} in the spouted bed.

For the two kinds of particles, PP and PA particles, have not only a different density but also a different dielectric constant (1.5 for PP, and 2.5 for PA). The particle density related to the fluidization behavior, and the dielectric constant related to the surface charge further. Van Laer's research[24] pointed out that the effect of dielectric constant and size of the beads on plasma

behavior in a packed bed DBD reactor utilizing a fluid model. The electric field was enhanced with the increase of particle dielectric constant. Due to the relatively high dielectric constant of PA particle, the electric field between the particle gap is higher, but the electric field inside the PA particle is lower than PP particle. On the other hand, the enhancement of the electric field with PP particles with a low dielectric constant is limited, which leads to the discharge flowing through the particle gap smoothly. It gives the reason that the enhancement of particle velocity is higher for the high percentage of PP particles in the mixture of PP and PA particles than the low percentage of PP particles.

5.4 Summary

This paper investigates the fluid dynamics of particles changed by plasma irradiation in an AC-DBD plasma-enhanced 2D spouted bed reactor, which lays a foundation for further research in chemical processes. This research extends our knowledge on the effect of plasma irradiation on the fluid dynamics in this combination system. Conclusions are presented as follows.

Firstly, the velocity profile of solid particles changed with the plasma irradiation in the plasma-enhanced spouted bed. The high particle velocity area, which showed at the upper part upon the plasma inlet, was improved with 7 kV applied voltage. With the plasma irradiation, the vertical velocity of particles was improved significantly despite along the longitudinal or lateral direction. The highest enhancement appeared when the gas velocity just exceeded the u_{ms}. However, the enhancement of particle velocity was not increased with the gas velocity. We assumed that the two electric fields presented in the system, which were the external electric field and the field by ion accumulation charges on the particle surface, resulted in the enhancement of

particle velocity. Besides, the electron temperature of plasma had been declined with the addition of particles.

Secondly, the influence on the particle velocity was different from particle type since the plasma irradiation. The $V_{y\text{-max}}$ of particles was enhanced with 7 kV applied voltage in most cases for PP and PA particles. However, the enhancement of $V_{y\text{-max}}$ for PA particles was less than that of PP particles due to the different particle density and dielectric constant. The values of $V_{y\text{-max}}$ were enhanced with a high percentage of PP particles addition in the mixture of PP particles and PA particles.

The plasma irradiation effected on the fluid dynamics of particles in the spouted bed. In consideration of the fluidization of particles and the effective utilization of the active states in the electric field for the particle applications, we must control a good fluidization behavior (gas velocity just exceeded the u_{ms}) in the system which is related to the proper gap size between solid particles.

5.5 References

[1].T. C. Corke, M. L. Post, and D. M. Orlov, "SDBD plasma enhanced aerodynamics: concepts, optimization and applications," Prog. Aerosp. Sci., vol. 43, no. 7–8, pp. 193–217, 2007.

[2].A. Komuro et al., "Multiple control modes of nanosecond-pulse-driven plasma-actuator evaluated by forces, static pressure, and PIV measurements," Exp. Fluids, vol. 59, no. 8, pp. 1–19, 2018.

[3].C. L. Enloe et al., "Mechanisms and Responses of a Dielectric Barrier Plasma Actuator:

Geometric Effects," AIAA J., vol. 42, no. 3, pp. 595–604, 2004.

[4].Z. A. Syed, "Computational modelling of Dielectric Barrier Discharge Plasma Actuators for Aerospace Flow control applications," master thesis, p. 92, 2016.

[5].Y. Li, X. Zhang, and X. Huang, "The use of plasma actuators for bluff body broadband noise control," Exp. Fluids, vol. 49, no. 2, pp. 367–377, 2010.

[6].Y. Sung, W. Kim, M. G. Mungal, and M. A. Cappelli, "Aerodynamic modification of flow over bluff objects by plasma actuation," Exp. Fluids, vol. 41, no. 3, pp. 479–486, 2006.

[7].X.-L. Zhao, S.-Q. Li, G.-Q. Liu, Q. Song, and Q. Yao, "Flow patterns of solids in a two-dimensional spouted bed with draft plates: PIV measurement and DEM simulations," Powder Technol., vol. 183, no. 1, pp. 79–87, Mar. 2008.

[8].S. van Buijtenen, M. Börner, N. G. Deen, S. Heinrich, S. Antonyuk, and J. A. M. Kuipers, "An experimental study of the effect of collision properties on spout fluidized bed dynamics," Powder Technol., vol. 206, no. 1–2, pp. 139–148, 2011.

[9].B. Singh, L. K. Rajendran, M. Giarra, P. P. Vlachos, and S. P. M. Bane, "Measurement of the flow field induced by a spark plasma using particle image velocimetry," Exp. Fluids, vol. 59, no. 12, pp. 1–15, 2018.

[10].Lai, V. Petrov, and J. E. Foster, "Understanding Plasma-Liquid Interface Instabilities Using Particle Image Velocimetry and Shadowgraphy Imaging Methods," IEEE Trans. Plasma Sci., vol. 46, no. 4, pp. 875–881, 2018.

[11].Meyer, A. Bück, and E. Tsotsas, "Determination of particle exchange rates at over-flow weirs in horizontal fluidised beds by particle tracking velocimetry," Particuology, vol. 32, pp. 1–9,

2017.

[12].T. Tsuji, T. Miyauchi, S. Oh, and T. Tanaka, "Simultaneous Measurement of Particle Motion and Temperature in Two-Dimensional Fluidized Bed with Heat Transfer," vol. 28, no. 28, pp. 167–179, 2010.

[13].A. Mychkovsky, D. Rangarajan, and S. Ceccio, "LDV measurements and analysis of gas and particulate phase velocity profiles in a vertical jet plume in a 2D bubbling fluidized bed: Part I: A two-phase LDV measurement technique," Powder Technol., vol. 220, pp. 55–62, Apr. 2012.

[14].G.-Q. Liu, S.-Q. Li, X.-L. Zhao, and Q. Yao, "Experimental studies of particle flow dynamics in a two-dimensional spouted bed," Chem. Eng. Sci., vol. 63, no. 4, pp. 1131–1141, Feb. 2008.

[15].S. Z. Li, W. T. Huang, and D. Wang, "The effect of gas flow on argon plasma discharge generated with a single-electrode configuration at atmospheric pressure," Phys. Plasmas, vol. 16, no. 9, 2009.

[16].P. Borra, "Nucleation and aerosol processing in atmospheric pressure electrical discharges: Powders production, coatings and filtration," J. Phys. D. Appl. Phys., vol. 39, no. 2, 2006.

[17].A. Science, "Triboelectrification of kcl and zns particles in approximated exoplanet environments," 2018.

[18].Zhang et al., "Needle-array to Plate DBD Plasma Using Sine AC and Nanosecond Pulse Excitations for Purpose of Improving Indoor Air Quality," Sci. Rep., vol. 6, no. January, pp. 1–14, 2016.

[19].C. J. Heijmans, F. M. J. H. Van De Wetering, and S. Nijdam, "The effect of single-particle charge limits on charge distributions in dusty plasmas," J. Phys. D. Appl. Phys., vol. 49, no. 38, p. 95201, 2016.

[20].J. H. Byeon et al., "Collection of submicron particles by an electrostatic precipitator using a dielectric barrier discharge," J. Aerosol Sci., vol. 37, no. 11, pp. 1618–1628, 2006.

[21].Michielsen et al., "CO2dissociation in a packed bed DBD reactor: First steps towards a better understanding of plasma catalysis," Chem. Eng. J., vol. 326, pp. 477–488, 2017.

[22].ZHANG, X. BIAN, Q. CHEN, F. LIU, Z. LIU, "Diagnosis of Methane Plasma Generated in an Atmospheric Pressure DBD Micro-Jet by Optical Emission Spectroscopy," CHIN. PHYS. LETT., vol. 35203, 2009.

[23].K. Van Laer and A. Bogaerts, "Fluid modelling of a packed bed dielectric barrier discharge plasma reactor," Plasma Sources Sci. Technol., vol. 25, no. 1, p. 15002, 2015.

[24].K. Van Laer and A. Bogaerts, "How bead size and dielectric constant affect the plasma behaviour in a packed bed plasma reactor: A modelling study," Plasma Sources Sci. Technol., vol. 26, no. 8, 2017.

6. Conclusions

This thesis proposed a combination system of AC DBD plasma with a spouted bed reactor. Three kinds of researches have been done here. The fluidization behavior of fine behavior, the fluid dynamic of large particles, and the effect of particles on the plasma feature were investigated. Several conclusions can be obtained as follows.

Firstly, the pressure drop, u_{ms}, void fraction were detected in the process with the plasma irradiation in a 3D spouted bed to determine the fluidization behavior of fine particles. The void fraction of solid bed was enhanced, and the entire solid bed was expanded since a high voltage applied, which means the distance of particles improved. It resulted in the pressure drop of solid bed decreased, and u_{ms} declined by the enhancement of applied voltage irrespective of the static bed height and working gas (Ar and N_2). The emission intensity for Ar plasma species increased, and $\triangle P$ decreased with the enhancement of applied voltage before the gas flow rate reached u_{ms} point. It is consistent with the mechanism that the ionization of the working gas was the main reason for the variation in particle fluidization behavior.

Secondly, the optical emission spectral characteristics of Ar plasma and the effect of fluidization behavior of PP and BPP particles on the optical emission spectral characteristics of plasma were investigated. With the presence of Ar plasma irradiation, the pressure drops for PP particles were decreased but not for BPP particles. The emission spectra of Ar plasma had been changed significantly with the addition of particles. The emission spectrum of Ar I was enhanced with PP particles and declined with BPP particles. The emission intensities of Ar I lines were enhanced with the voltage applied regardless of the addition of particles. The changes in emission

intensity with flow rate were different in the cases of particles and non-particles. The emission intensity of plasma versus particle numbers was identified with fluidization behavior. The difference in color (absorption and reflection) and electrical conductivity (charge transfer rate) between BPP and PP particles may be resulting in the distinction on detected emission spectral data and pressure drop.

Then, we investigated the fluid dynamics changes and mechanism with plasma irradiation. With the plasma irradiation, vertical velocity was improved despite longitudinal or lateral direction. V_{y-max} of particles was enhanced with 7 kV applied voltage in most cases for PP and PA particles. The values of V_{y-max} were enhanced with a high percentage of PP added in the mixture of PP and PA particles. The difference of dielectric constant and density for PA and PP resulted in the changes in pressure drop changes and velocity profile for particles.

Our findings give the relationship between fluidization behavior and plasma optical characteristic. It suggests that a promotion of plasma emission intensity by particles fluidization (proper contact points and gap size) that might provide a viable source for the process such as in the process of plasmatic pollutant disposal with the catalysts. In the cases of different type of particles, the color of surface which related to the radiation feature affected the detected emission intensity of plasma. Besides, the electric features, electrical conductivity and dielectric constant, influenced on the difference of pressure drop with applied voltage and particle velocity profile, respectively. It is well accepted that a positive synergy effect between plasma irradiation and particle fluidization behavior.

Acknowledge

It is not possible to complete this thesis without assistance from so many people in my life. First of all. I want to thank my supervisor and professor, *Nobusuke Kobayashi*. Thank you so much for your support and guidance over the past three years. Not only for the support of the research but also daily care for an international student who lived in Japan. Due to your guidance on the way for research, I can form my thoughts on the thesis. Thank you so much give me so many opportunities to present at international and domestic conferences. I can feel so many changes from the first time I stood in front of professional researches until now. I feel lucky to have *Yoshinori Itaya* as a co-advisor. Your comments and insight on the experimental setup, data analysis, and public writing have been invaluable. I must thank *Akira Suami* for helping me to figure out so many tiny things in the lab. Thank Prof. *Kanbara* for supporting the plasma power equipment and advice for my research. To my master advisor at Nanjing Normal University, *Guilin Piao*, thanks for introducing me to engineering chemistry 7 years before, introducing me to Gifu University and becoming a friend over the years.

I thank all the friends in our lab. Because of you, *Bao, Arash and Zhang*, I can feel the research life is not boring for staying inside of the lab and I can feel the strong support from you. Thank the Japanese students in our lab, especially *Ono*, *Noguchi,* and *Okata,* thank you put up my poor Japanese and kindly teach me again and again. I know so much of the culture by so many friends from other countries here. More thanks are due to the friends I met here and my old friends in China, your support, understanding, care, and so much fun when we are together. It is an interesting life in Japan because of you. I must give a special thanks to my family and my

boyfriend. Your support, trust, care, share, and everything have been to be my lifetime wealth.